REPORT DOCUMENTATION PAGE

Form Approved
OMB No. 0704-0188

PLEASE DO NOT RETURN YOUR FORM TO THE ABOVE ADDRESS.

1. REPORT DATE *(DD-MM-YYYY)*	2. REPORT TYPE	3. DATES COVERED *(From - To)*
10-05-2010		

4. TITLE AND SUBTITLE
Dynamic Analysis of an Optical Laser Platform

5a. CONTRACT NUMBER

5b. GRANT NUMBER

5c. PROGRAM ELEMENT NUMBER

6. AUTHOR(S)
Roush, Angela Marie

5d. PROJECT NUMBER

5e. TASK NUMBER

5f. WORK UNIT NUMBER

7. PERFORMING ORGANIZATION NAME(S) AND ADDRESS(ES)

8. PERFORMING ORGANIZATION REPORT NUMBER

9. SPONSORING/MONITORING AGENCY NAME(S) AND ADDRESS(ES)
U.S. Naval Academy
Annapolis, MD 21402

10. SPONSOR/MONITOR'S ACRONYM(S)

11. SPONSOR/MONITOR'S REPORT NUMBER(S)
Trident Scholar Report no. 393 (2010)

12. DISTRIBUTION/AVAILABILITY STATEMENT
This document has been approved for public release; its distribution is UNLIMITED

13. SUPPLEMENTARY NOTES

14. ABSTRACT
In this project, Lagrange's equations of motion are derived for a visco-elastic, point-supported plate containing discrete masses, which is representative of an optical platform. The mechanical response of the optical platform is sought for free vibration, impact loading and the response imparted by two inertial actuators. All three of these responses are then analyzed with and without damping. A solution of these equations contains information pertaining to the plate's amplitude and frequency, analyzed in both time and frequency domains, which together computes the effect of jitter on the intensity of a directed energy beam at the target.

15. SUBJECT TERMS
Jitter, Lagrange's Equations, Viso-elastic, Actuators

16. SECURITY CLASSIFICATION OF:			17. LIMITATION OF ABSTRACT	18. NUMBER OF PAGES	19a. NAME OF RESPONSIBLE PERSON
a. REPORT	b. ABSTRACT	c. THIS PAGE		83	19b. TELEPHONE NUMBER *(Include area code)*

ABSTRACT

Optical beam pointing is a critical topic in the study of Directed Energy Weapons Systems. One of the main operational concerns with optical beam pointing is the effect of small vibratory motion, defined as jitter. Understanding jitter is important for minimizing the effect it has upon a directed energy beam's intensity at its target. In this project, Lagrange's equations of motion are derived for a visco-elastic, point-supported plate containing discrete masses, which is representative of an optical platform. The mechanical response of the optical platform is sought for free vibration, impact loading and the response imparted by two inertial actuators. All three of these responses are then analyzed with and without damping. A solution of these equations contains information pertaining to the plate's amplitude and frequency, analyzed in both time and frequency domains, which together computes the effect of jitter on the intensity of a directed energy beam at the target.

Keywords: jitter, Lagrange's equations, viso-elastic, actuators

ACKNOWLEDGMENTS

There are many individuals without whom this project would not have been possible. First and foremost, I would like to acknowledge the assistance of Professor Oscar Barton, who directed and guided me through the challenges of modeling, vibration analysis, and the world of MATHEMATICA®. Without his continued support and faith in me, this project would not have materialized. I am also grateful for CDR Watkins's assistance at the DEPS Symposium and his insight into the practical application of my project.

The work presented here is a part of a program of research into jitter control conducted at the United States Naval Academy funded by the Office of Naval Research. I would, therefore, like to thank the Office of Naval Research and the Department of Defense for their continued support.

TABLE OF CONTENTS

LIST OF TABLES

LIST OF FIGURES

PAGE

NOMENCLATURE

A	= amplitude
c	= damping coefficient
c_{cr}	= critical damping
E	= Elastic modulus (Young's modulus)
Hz	= cycles per second (Hertz)
I_{xx}, I_{yy}, I_{xy},…	= mass moment of inertia
k	= stiffness coefficient
m	= mass
N	= Force (Newton)
P	= matrix of eigenvectors
Pa	= Force per unit area (Pascal)
R	= Rayleigh's dissipation function
r(t)	= displacement in modal space with respect to time
S	= transformation matrix from modal space to original space
t	= time
T	= Period of oscillation
T	= Kinetic Energy
ζ	= damping ratio
V	= Spring Energy
ω_d	= damped natural frequency
ω_n	= natural frequency
ϕ	= phase

CHAPTER 1

INTRODUCTION AND BACKGROUND

1.1 Introduction

Directed energy systems have eluded researchers and engineers for decades due to the vast difficulties ranging from the basic physics of the system to modeling and system design. Advances in laser and control systems have proved fruitful towards solving these problems. Attention is now turning to other issues that affect the directed energy system. One such challenge is to gain a better understanding of induced structural vibrations on the mechanical response of the structure that contains the directed energy system. This vibration, termed jitter, has a measurable effect on the accuracy and intensity of the laser at its target. A model capable of simulating the motion of an optical platform in various scenarios would greatly assist in the understanding of jitter effects and the mechanics behind the structural support system of the laser.

1.2 Background

The optical laser system can be modeled as a multiple degree of freedom rigid body with attached discrete masses supported on visco-elastic springs. One approach is to model it as a flexible body and, due to the support conditions, include rigid body modes. Work on the vibration of deformable plates is mature and only an overview is presented here.

Cox and Boxer [1] provided one of the early contributions to this topic and discussed the vibration of a point supported plate at its corners and free edge boundaries elsewhere. Both rotary inertia and shear effects were neglected for the plate. A finite difference approach was used to solve the governing differential equation, and provided mode shapes and frequencies for

both square and rectangular plates. Amba-Rao [2] studied the vibration of a simply-supported rectangular plate carrying a concentrated mass and presents a closed-form solution for the frequencies and mode shapes. To develop the formulae for the frequencies, the transverse displacement was represented as a double infinite sine series. Kerstens [3] incorporated a modal constraint method to solve the problem of vibration of a rectangular plate supported arbitrarily. The modal constraint approach used the principle of minimum potential energy, which included virtual work done by homogeneous boundary conditions. The point supports were represented through the virtual work by a homogenous boundary condition formed by finite constraints as point supports. A Lagrange multiplier was used to represent the unknown forces. The use of the Rayleigh-Ritz method continues to be a common approach for solving the eigenvalue problem associated with plate vibration. Of particular interest was the selection of basis function used in the analysis. Lee and Lee [4] incorporated a new class of admissible functions to study the vibration of elastically point supported plates. The basis function corresponded to a similarly supported beam under point loads. Singularity functions were used to completely describe the equation defining the elastic curve. Normalized frequencies were presented for a plate simply supported on all sides and as a function of support location as well as elastic support stiffness. Kim and Dickerson [5] incorporate orthonormal polynomials as the basis functions in the Rayleigh-Ritz method to study the vibration of point supported plates with a combination of simply-supported and clamped edge conditions. The orthronormal set was constructed using the Gramm-Schmidt process. Kocaturk et al. [6] considered the dynamic response of a thin orthotropic plate supported on viscoelastic supports, which all had stiffness and damping properties. The plate was subjected to harmonic input at its center and supported added masses. The arrangement of the masses was placed symmetrically along the diagonals of the plate. A

Ritz method was used to compute the eigenparameters presented in the Lagrange's equation of motion. Results were presented for several material constituents and considered symmetric modes of vibration consistent with geometry. The authors also presented results for the force transmissibility as a function of plate material properties and added mass.

Of particular interest was experimental work that had been done in this area of investigation. Although not as voluminous as numerical and analytical work, several contributions were noteworthy in literature. Nieves [7] et al used laser interferometry to identify the flexural vibrations of thick isotropic plate. The technique was said to consist solely of out-of-plane displacement flexural modes. Analytical results from the Ritz method were used as comparisons for accuracy. A Mindlin plate theory was the basis for the analytical study presented. Lee and Kam [8] considered the effect of elastic-edge supports on the vibration of composite plates as a means of determining the mechanical properties of a plate. Impulse data provided the necessary frequencies to extract the mechanical properties.

Rigid body mechanics offered a much more suitable alternative in light of design, fabrication and construction of mounted systems aboard ships and aircraft. In this approach, kinematic equations predicted motion leading to an understanding of the vibration response.

1.3 Approach

The analysis of a vibrating system usually involved mathematical modeling, derivation of the governing equations, solution of the equations, and interpretation of the results. A brief summary of each step follows. More detailed descriptions are included in chapters (2-6).

Step 1: Mathematical Modeling

The purpose of mathematical modeling is to represent all the important features of the system for the purpose of deriving analytical equations governing the system's behavior. The mathematical model may be linear or nonlinear.

Step 2: Derivation of Governing Equations

Several approaches are commonly used to derive the governing equations of motion. Among them are Newtonian Mechanics, Hamilton's Principle, the Principle of Virtual Work, and Lagrange's Equation. When only single degree systems are considered, Newton's law is useful, but in more practical problems with many degrees of freedom, energy considerations can be combined with the concepts of virtual work to produce Lagrange's equations. Lagrange's equations provide an energy-based alternative to summing forces to derive equations of motion and are therefore used in this project.

Step 3: Solution of the Governing Equations

The equations of motion must be solved to find the response of the vibrating system. Depending on the nature of the problem, one of the following techniques may be used to find the solution: standard methods of solving differential equations, Laplace transform methods, matrix methods, and numerical methods. The resulting problem for the vibration of the rigid problem is an eigenvalue problem. Modal analysis is one approach to solve the associated eigenvalue problem using vector transformations.

Step 4: Interpretation of the Results

The solution of the governing equations gives the displacements, velocities, and accelerations of the system's various masses. These results can be analyzed for possible design implications. Accuracy of a model is determined by how well the solution of the

governing equations of motion predict the observed behaviors of the system presented in experimental results.

1.4 Objectives

The objectives of this study were as follows:

1. to model the optical platform as a rigid plate supported by elastic springs containing discrete masses
2. to determine an exact differential of motions representing the kinematic model
3. to determine its mechanical response for free vibration, impact analysis, and forced vibration.
4. to incorporate MATHEMATICA as the computation tool for analysis of the mechanical response-based method to analytically solve for the equations of motion

CHAPTER 2

MODELING

2.1 Introduction

This chapter introduces a brief overview of methods available to develop the equation of motions for rigid point supported plates in order to provide a framework of vibration; that is, to represent the physical problem mathematically. Differential equations governing the forced vibration of a rigid point supported plate were then developed using Lagrange's equation. By defining the plate's motion in terms of generalized displacement parameters, one captured all six degrees of freedom in terms of three translations and three rotations.

Methods to represent or model physical problems all have their roots in dynamic equilibrium or Newton's 2nd Law. For rigid bodies, two vectors equations given as

$$\begin{aligned} \sum \overline{F} &= m\,\overline{a}_G \\ \sum M_G &= I_p \alpha_p \end{aligned} \tag{2.1}$$

where p takes on indices of $x, y, or\ z$. Here $\overline{a}_G$ is the acceleration at the center of mass, m is the mass, I_p is the mass moment of inertia about the p^{th} axis, and α the angular acceleration about the p^{th} axis. As the system became more complicated, establishing the vector required relationships in Newton's approach became increasingly difficult and required a more concise approach.

As an alternative to this vector-based formulation, the method of principle virtual work was a scalar-based approach providing a shift in formulation from a Newtonian to a Lagrangian approach. Problems in dynamics and vibration required introducing d'Alembert principle, since the principle of virtual work was essentially a variation principle for problems in statics coordinates used to define the degrees of freedom for the system. Stated simply

The total work performed by the effective forces through infinitesimal virtual displacements compatible with the system constrains is zero.

and mathematically is represented as

$$\sum \left(\bar{F}_i - \dot{\bar{p}}_i\right) \cdot \delta \bar{r}_i = \bar{0} \tag{2.2}$$

In equation 2.2, δr_i is a virtual displacement compatible with the constraints on the system. When deriving equations of motion, independent coordinates were preferred over system position variables, which lead to the definition of generalized coordinates and Lagrange's Equations of Motion. A complete derivation of Lagrange's equations can be found in [9]. Here it is stated as

$$\frac{d}{dt}\left(\frac{\partial T}{\partial \dot{q}_i}\right) - \frac{\partial T}{\partial q_i} + \frac{\partial R}{\partial \dot{q}_i} + \frac{\partial V}{\partial q_i} = Q_i \tag{2.3}$$

where T is the system's kinetic energy, V, the system's potential energy, and R is defined as Rayleigh's dissipation function and represents energy loss due to damping. Also q_i's are generalized displacements and Q_i's are the corresponding generalized forces. The term generalized is used to described translations or rotations as well as forces or moments.

2.2 Kinematic Model Development

Lagrange's equation of motion was the preferred approach to develop the differential equations of motion for the point supported plate. To do so required a definition of the generalized displacements, and provided the starting point of kinematic analysis.

Figure 2.1 shows the experimental setup of the optical platform and all of its required instrumentation. Two inertial actuators were mounted to provide forced motion in the vertical direction as well as to create angular rotations about the three cartesian axes. As a consequence of the induced motions, displacements in the x and z directions were produced and accounted for

in the kinematic model. Other elements included mounted brackets for optical sensors, laser beam, and sensors themselves. Each element added mass and hence affected the mechanical response of the optical platform system. Vibration isolators provided a mounting base for each of elastic four springs.

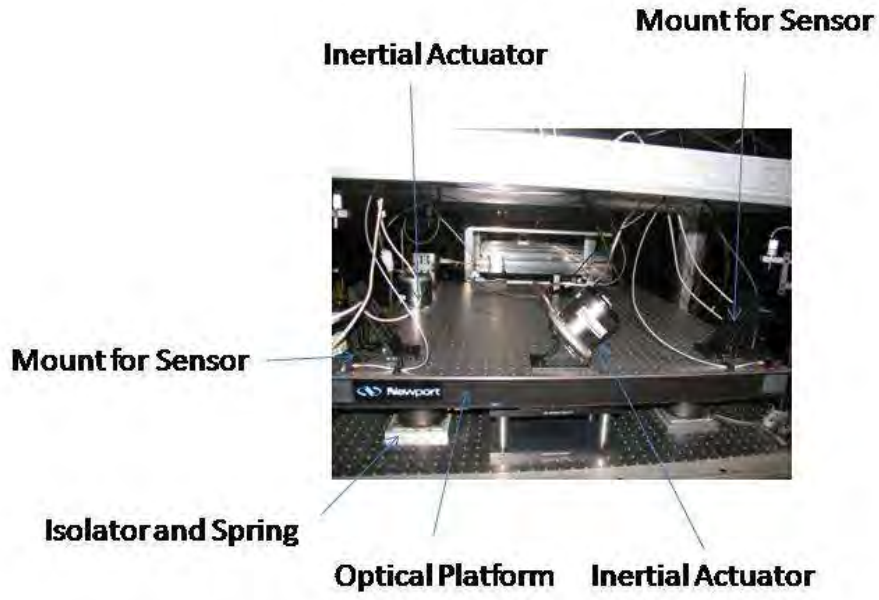

Figure 2.1: Experimental Setup

As such, the system was modeled as an elastically point supported plate containing discrete masses. The platform was taken to be a rigid body, which simulated the construct of the actual system in operation.

The developed kinematic model consisted of superimposed displacement in the x, y, and z directions. Three two-dimensional representations were used to develop the total displacement expressions u{y,z}, v{x,z}and w{x,y} for the system consisting of a rigid platform and any number of discrete masses, depicted below as the k^{th} masses. The cartesian coordinate system had been located at the geometric center of the plate, its centroid, and provided the means necessary to establish a relative position vector expression to locate movement in terms of

displacements given by $\{u_0, v_0, w_0\}$ and angular rotations given by $\{\theta_x, \theta_y, \theta_z\}$. The procedure used to develop the displacement expression is presented in equations (2.4) through (2.9). First consider figure 2.2, which shows kinematics relationships for the x-y plane. All terms were considered positive. The centroid displaced by u_0 and v_0, which represented the translation of the center of gravity. In this plane, θ_z represented a positive rotation, and elements located in the positive x-y quadrant experienced displacements given by

$$\bar{r}_{k/G} = \{x - x\,Cos(\theta_z) - y\,Sin(\theta_z)\}\hat{i} + \{x\,Sin(\theta_z) - (y - y\,Cos(\theta_z))\}\hat{j} \tag{2.4}$$

Combining translations and rotations provided

$$\bar{r}_k = \{u_0 + x - x\,Cos(\theta_z) - y\,Sin(\theta_z)\}\hat{i} + \{v_0 + x\,Sin(\theta_z) - (y - y\,Cos(\theta_z))\}\hat{j} \tag{2.5}$$

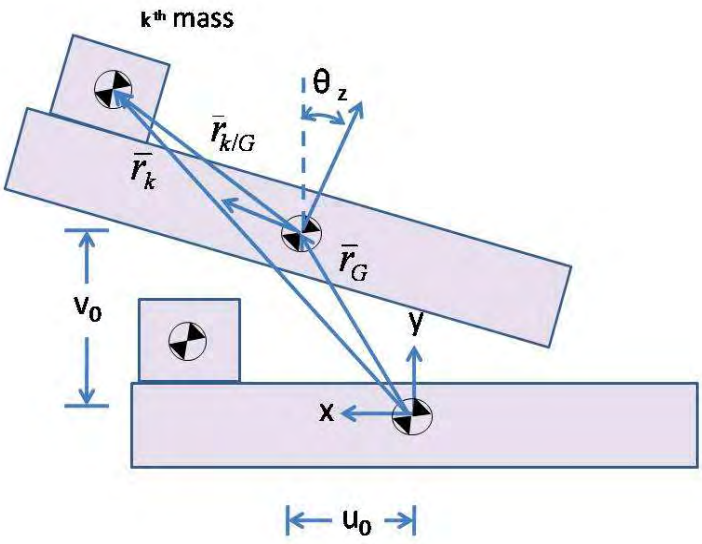

Figure 2.2: Free Body Diagram in X-Y Plane

The amplitude of motion experienced by the plate and its discrete elements were on the order of micrometers and micro-radians. Using a small angle assumption resulted in

$$\bar{r}_k = \{u_0 - y\,\theta_z\}\hat{i} + \{v_0 + x\,(\theta_z)\}\hat{j} \tag{2.6}$$

Referring to figure 2.3 and making similar assumptions of displacement and rotation amplitudes, the position vector in the y-z plane was computed as

$$\bar{r}_k = \{v_0 - z\,\theta_x\}\,\hat{j} + \{w_0 + y\;\theta_x\}\,\hat{k} \tag{2.7}$$

The final contribution was determined by referring to figure 2.4, which represented motion in the x-z plane. This became

$$\bar{r}_k = \{u_0 + x + z\,\theta_y\}\,\hat{i} + \{w_0 - x\,\theta_y + z\}\,\hat{k} \tag{2.8}$$

The total position vector now was determined by summing equations (2.5) to (2.8) producing

$$\bar{r}_k = u\{y,z,t\}\,\hat{i} + v\{x,z,t\}\,\hat{j} + w\{x,y,t\}\,\hat{k} \tag{2.9}$$

where

$$\begin{aligned} u(y,z,t) &= u_0(t) + z\theta_y(t) - y\theta_z(t) \\ v(x,z,t) &= v_0(t) - z\theta_x(t) + x\theta_z(t) \\ w(x,y,t) &= w_0(t) - x\theta_y(t) + y\theta_x(t) \end{aligned} \tag{2.10}$$

Care was taken to not account for contributions more than once.

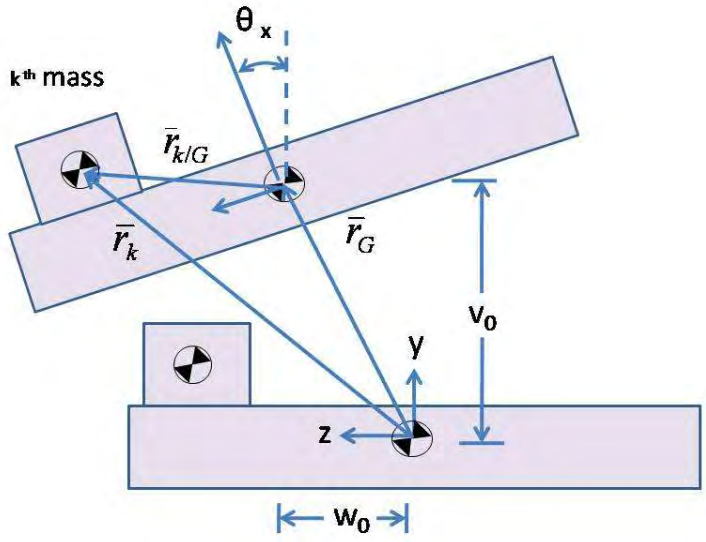

Figure 2.3: Free Body Diagram in Y-Z Plane

Equation (2.10) is the displacement equation required for Lagrange's equation.

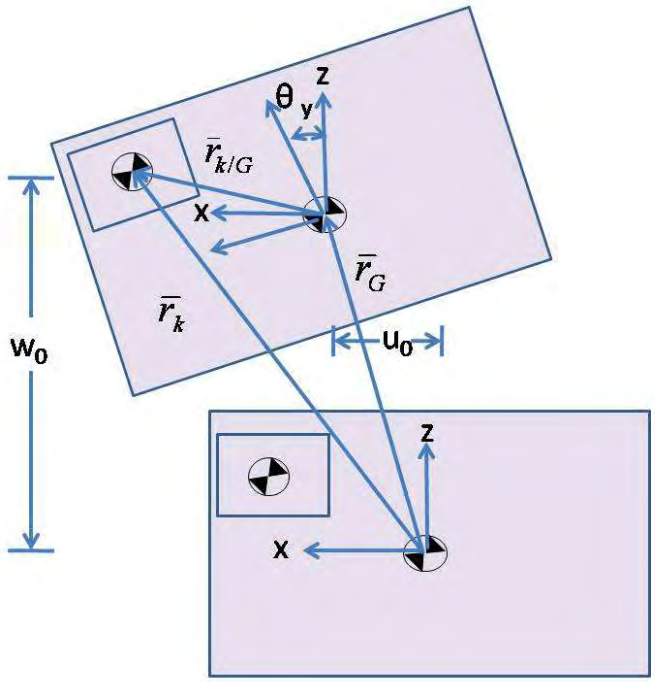

Figure 2.4: Free Body Diagram in X-Z Plane

2.3 Dynamic Model Development

Figure 2.5 shows a planar view of dynamic model that represented the optical platform. The actual system had two mounted actuators oriented 45˚ relative to the horizontal. Each inertial actuator had been modeled as an equivalent mass-spring-damper system with stiffness k_{si} and damping coefficient c_{si} . Here m_{top} was the portion of the actuator's mass in motion and m_{base} was the remaining mass for the actuator. Discrete masses were represented by the k^{th} mass. Experimental testing of the system's support springs revealed that, although geometrically similar, measured spring stiffnesses could vary by as much as 30%. To account for this variation, spring stiffnesses and damping coefficients were all labeled differently as k_i and c_i .

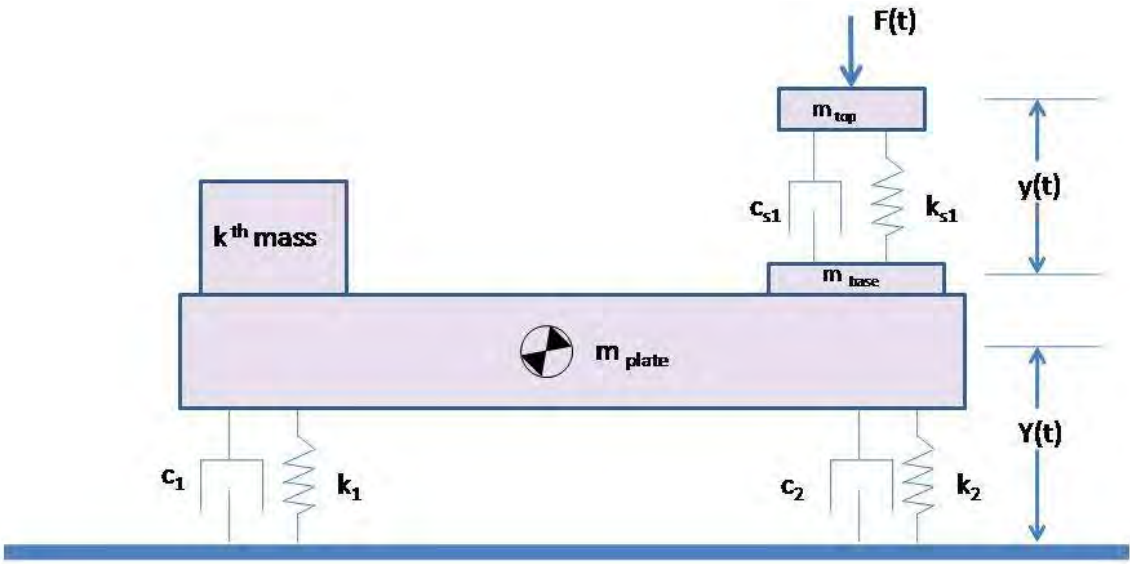

Figure 2.5: Side view of a Platform with Discrete Mass and Actuator

Expression for the kinetic energy, potential energy and Rayleigh Dissipation function for each inertial actuator were given by

$$T_{actuators} = \frac{1}{2} m_{s1}(\dot{u}_{s1}^2 + \dot{v}_{s1}^2) + \frac{1}{2} m_{s2}(\dot{v}_{s2}^2 + \dot{w}_{s2}^2) \tag{2.11}$$

$$\begin{aligned} V_{actuators} &= \frac{1}{2} k_{s1}[(u_{s1} - u\{y_{s1}, z_{s1}\})^2 + (v_{s1} - v\{y_{s1}, z_{s1}\})^2 + w\{y_{s1}, z_{s1}\})]^2 \\ &+ \frac{1}{2} k_{s2}[u\{y_{s2}, z_{s2}\}^2 + (v_{s2} - v\{y_{s2}, z_{s2}\})^2 + (w_{s2} - w\{y_{s2}, z_{s2}\})]^2 \end{aligned} \tag{2.12}$$

$$\begin{aligned} R_{actuators} &= \frac{1}{2} c_{s1}[(\dot{u}_{s1} - \dot{u}\{y_{s1}, z_{s1}\})^2 + (\dot{v}_{s1} - \dot{v}\{y_{s1}, z_{s1}\})^2 + \dot{w}\{y_{s1}, z_{s1}\})^2] \\ &+ \frac{1}{2} c_{s2}[\dot{u}\{y_{s2}, z_{s2}\})^2 + (\dot{v}_{s2} - \dot{v}\{y_{s2}, z_{s2}\})^2 + (\dot{w}_{s2} - \dot{w}\{y_{s2}, z_{s2}\})^2] \end{aligned} \tag{2.13}$$

and expressions for the kinetic energy, potential energy, and Rayleigh's Dissipation function for the plate were given as

$$\begin{aligned} T &= \frac{1}{2} \sum_{i=1}^{N} m_i(\dot{u}_i^{\,2} + \dot{v}_i^{\,2} + \dot{w}_i^{\,2}) + \frac{1}{2} \iiint (\dot{u}_i^{\,2} + \dot{v}_i^{\,2} + \dot{w}_i^{\,2}) dm \\ R &= \frac{1}{2} \sum_{i=1}^{4} c_i(\dot{u}_i^{\,2} + \dot{v}_i^{\,2} + \dot{w}_i^{\,2}) \\ V &= \frac{1}{2} \sum_{i=1}^{4} k_i(u_i^{\,2} + v_i^{\,2} + w_i^{\,2}) \end{aligned} \tag{2.14}$$

Substitution of equations (2.12) through (2.15) into (2.3) yielded the coupled equations of motion represented in matrix form as

$$\begin{bmatrix} [m_s]_{(4x4)} & [0]_{(4x6)} \\ [0]_{(6x4)} & [m_p]_{(6x6)} \end{bmatrix} \begin{Bmatrix} \{\ddot{q}_s\}_{(4x1)} \\ \{\ddot{q}_p\}_{(6x1)} \end{Bmatrix} + \begin{bmatrix} [c_s]_{(4x4)} & [c_{ps}]_{(4x6)} \\ [c_{sp}]_{(6x4)} & [c_p]_{(6x6)} \end{bmatrix} \begin{Bmatrix} \{\dot{q}_s\}_{(4x1)} \\ \{\dot{q}_p\}_{(6x1)} \end{Bmatrix} + \begin{bmatrix} [k_s]_{(4x4)} & [k_{ps}]_{(4x6)} \\ [k_{sp}]_{(6x4)} & [k_p]_{(6x6)} \end{bmatrix} \begin{Bmatrix} \{q_s\}_{(4x1)} \\ \{q_p\}_{(6x1)} \end{Bmatrix} = \begin{Bmatrix} \{Q_s\}_{(4x1)} \\ \{0\}_{(6x1)} \end{Bmatrix} \tag{2.15}$$

The explicit equations were quite lengthy and can be referenced in Appendix A -1 and appendix A-2, which provide sub-matrices used in eqn.(2-15). The above subscripts s and p in eqn. (2.16) correspond to the shaker and plate, respectively. Also, the vectors of generalized coordinates are defined as

$$\{q_s\} = \begin{Bmatrix} u_{s1} \\ v_{s1} \\ v_{s2} \\ w_{s2} \end{Bmatrix} \qquad \{q_p\} = \begin{Bmatrix} u_0 \\ v_0 \\ w_0 \\ \theta_x \\ \theta_y \\ \theta_z \end{Bmatrix} \tag{2.16}$$

This set of equations is coupled both statically and dynamically, representing damped forced vibration analysis. Initial condition must be appended to eqn (2.15), which consisted of initial displacement and initial velocities.

Equation (2.15) was specialized based upon the type of vibration analysis investigated. Initial conditions can also be presented. For free damped vibration analysis, eqn. (2-15) reduced to

$$[m_p]_{(6x6)} \{\ddot{q}_p\}_{(6x1)} + [c_p]_{(6x6)} \{\dot{q}_p\}_{(6x1)} + [k_p]_{(6x6)} \{q_p\}_{(6x1)} = \{0\}_{(6x1)} \tag{2.17}$$

with initial conditions of

$$\{q_p\} = \begin{Bmatrix} u_0(0) \\ v_0(0) \\ w_0(0) \\ \theta_x(0) \\ \theta_z(0) \\ \theta_z(0) \end{Bmatrix} \qquad \{\dot{q}_p\} = \begin{Bmatrix} 0 \\ 0 \\ 0 \\ 0 \\ 0 \\ 0 \end{Bmatrix} \tag{2.18}$$

Although initial velocity was possible, only displacement conditions were presented to reflect the reality of inducing such initial conditions in a laboratory setting. Equation (2.17) also governed impact analysis. However, the accompanying set of initial conditions were

$$\{q_p\} = \begin{Bmatrix} 0 \\ 0 \\ 0 \\ 0 \\ 0 \\ 0 \end{Bmatrix} \qquad \{\dot{q}_p\} = \begin{Bmatrix} 0 \\ v_0(0^+) \\ 0 \\ \dot{\theta}_x(0^+) \\ 0 \\ \dot{\theta}_z(0^+) \end{Bmatrix}$$

These initial conditions were computed from changes in both linear and angular momentum of the plate just before impact and immediately after impact, given by

$$\begin{aligned} \int_{0^-}^{0^+} F dt &= mv(0^+) - mv(0^-) \\ \int_{0^-}^{0^+} M_x dt &= I_{xx}\dot{\theta}_x(0^+) - I_{xx}\dot{\theta}_x(0^-) \\ \int_{0^-}^{0^+} M_z dt &= I_{zz}\dot{\theta}_z(0^+) - I_{zz}\dot{\theta}_z(0^-) \end{aligned} \tag{2.19}$$

The impact location did have an effect on the initial conditions. A plate impacted in its center resulted only in changes in linear momentum and not angular momentum.

Finally, steady-state forced vibration analysis for the system was considered. No initial conditions were required.

CHAPTER 3

MODAL ANALYSIS

3.1 Modal Analysis

In this chapter an overview of the solution strategy, modal analysis, is presented and used to solve the mechanical response in light of the complicated structure of the governing equations. The equations of dynamic equilibrium were coupled both statically and dynamically and, with the presence of damping, did not render a decoupled system unless certain conditions existed between the stiffness, damping and mass matrices.

There were many ways to decouple eqn. (2.15) based upon the existing type coupling construct. Consider the two-degree of freedom, coupled system, given by

$$\begin{bmatrix} m_{11} & m_{12} \\ m_{12} & m_{22} \end{bmatrix} \begin{Bmatrix} \ddot{x}_1 \\ \ddot{x}_2 \end{Bmatrix} + \begin{bmatrix} c_{11} & c_{12} \\ c_{12} & c_{22} \end{bmatrix} \begin{Bmatrix} \dot{x}_1 \\ \dot{x}_2 \end{Bmatrix} + \begin{bmatrix} k_{11} & k_{12} \\ k_{12} & k_{22} \end{bmatrix} \begin{Bmatrix} x_1 \\ x_2 \end{Bmatrix} = \begin{Bmatrix} F_1 \\ F_2 \end{Bmatrix} \tag{3.1}$$

or in matrix form as

$$[m]\{\ddot{x}\} + [c]\{\dot{x}\} + [k]\{x\} = \{F\} \tag{3.2}$$

Now simplify the equations to consider an undamped problem with $m_{12} = m_{21} = 0$, a system coupled by virtue of the stiffness elements only. Since the mass matrix is now diagonal, a coordinate transformation, defined as

$$\{q\} = [m]^{\frac{1}{2}}\{x\} \tag{3.3}$$

produces

$$[m][m]^{-\frac{1}{2}}\{\ddot{q}\} + [k][m]^{-\frac{1}{2}}\{q\} = \{F\} \tag{3.4}$$

Pre-multiplying eqn.(3.3) by $[m]^{-\frac{1}{2}}$ yields

$$[I]\{\ddot{q}\} + [\hat{k}]\{q\} = \{\hat{F}\} \tag{3.5}$$

where

$$[I] = [m]^{-\frac{1}{2}}[m][m]^{-\frac{1}{2}}$$
$$[\hat{k}] = [m]^{-\frac{1}{2}}[k][m]^{-\frac{1}{2}} \quad (3.6)$$
$$\{\hat{F}\} = [m]^{-\frac{1}{2}}\{F\}$$

In eqn. (3.5), $[\hat{k}]$ is the mass normalized stiffness matrix and [I] is the identity matrix. The modal transformation matrix is accomplished by determining the matrix of eigenvectors corresponding to eqn. (3.5), identified here as [P], defining a modal coordinate system {r} through the transformation of {q} = [P]{r}, and incorporating this transformation into eqn. (3.4). Doing so produces

$$[I][P]\{\ddot{r}\} + [\hat{k}][P]\{r\} = \{\hat{F}\} \quad (3.7)$$

and pre-multiplying by $[P]^T$ yields a decoupled system of equations of

$$\{\ddot{r}\} + [\tilde{k}]\{r\} = \{\tilde{F}\} \quad (3.8)$$

where

$$[\tilde{k}] = [P]^T[\hat{k}][P]$$
$$\{\tilde{F}\} = [P]^T\{\hat{F}\} \quad (3.9)$$

Eqn (3.8) was solved directly. The solution to the required problem was obtained after the solution in modal space was transformed back to the original coordinate system using the modal transformation given by

$$\{x\} = [S]\{r\} \quad (3.10)$$

where

$$[S] = [m]^{-\frac{1}{2}}[P] \quad (3.11)$$

Now consider the un-damped problem, but one that is coupled both statically and dynamically; that is, one with fully populated mass and stiffness matrices. Using the

transformation defined through eqn. (3.3) is not the most efficient method for this type of problem. Rather, a Cholesky Decomposition is the preferred strategy.

The Cholesky Decomposition, L, produces a lower triangular matrix that satisfies the matrix product of [m] = [L][L]^{T}. Most of the context presented will hold for this coordinate transformation, defined as

$$\{q\} = [L^T]\{x\} \tag{3.12}$$

which produces

$$[m][L^T]^{-1}\{\ddot{q}\} + [k][L^T]^{-1}\{q\} = \{F\} \tag{3.13}$$

Pre-multiplying eqn.(3.7) by $[L]^{-1}$ yields

$$[I]\{\ddot{q}\} + [\hat{k}]\{q\} = \{\hat{F}\} \tag{3.14}$$

where

$$\begin{aligned} [I] &= [L]^{-1}[m][L^T]^{-1} \\ [\hat{k}] &= [L]^{-1}[k][L^T]^{-1} \\ \{\hat{F}\} &= [L]^{-1}\{F\} \end{aligned} \tag{3.15}$$

The eigenvector matrix [P] can now be determined, and the modal transformation matrix [S] required is defined through

$$\{x\} = [S]\{r\} \tag{3.16}$$

where

$$\begin{aligned} [S] &= [L^T]^{-1}[P] \\ [S]^{-1} &= [P^T][L^T] \end{aligned} \tag{3.17}$$

Damping complicated the process in several ways. First, it was challenging to measure, and secondly, with damping present, there were no assurances that the matrix of eigenvectors would

diagonalize the damping matrix, thus decoupling the system. Caugley and O'Kelly [13] have shown exactly that.

$$\begin{aligned}[k][m]^{-1}[c] &= [c][m]^{-1}[k] \\ [m][k]^{-1}[c] &= [c][k]^{-1}[m] \\ [m][c]^{-1}[k] &= [k][c]^{-1}[m]\end{aligned} \tag{3.18}$$

Whenever eqn. (3.18) does not hold, then a proportional damping model is recommended in which the damping matrix [c] can be expressed as a linear combination of the mass and stiffness matrix gven by

$$[c] = \alpha[M] + \beta[k] \tag{3.19}$$

Constants α and β were selected to produce a desired damping ratio, based upon experimental results or design considerations.

Since the damping is mode dependent, the damping ratio is given as

$$\zeta_i = \frac{\alpha}{2\omega_i} + \frac{\beta\omega_i}{2} \tag{3.20}$$

CHAPTER 4

FREE VIBRATION

4.1 Introduction

This chapter presents the free vibration analysis of the system. Equation (2.17) and (2.18) were solved based upon the discussion in chapter 3. Required in the analysis were all of the system properties. The mass or the platform and discrete elements were weighted and recorded. Data from the manufacturer of the support springs indicated the same spring stiffness. However, experimental results for the spring stiffnesses indicated stiffness coefficients that varied as much as 30 percent. Free vibration case studies were investigated, which vary spring stiffness, discrete mass amount and location, and in the case of damping, damping ratios. Target displacement plots were plots that map the plate's motion onto a plane located a set distance away from the center of the plate, and presented a visual viewpoint of the platform's local motion. All results computed herein were performed using MATHEMATICA®.

Figure 4.1 shows the topology of stiffness and masses used in the vibration studies. The coordinate system was placed at the centroid. The plate had geometry of 36 in x 36 in x 2 in. with a density of 0.016 lb/in^3. The springs were mounted at fixed coordinates as listed in Table 4.1.

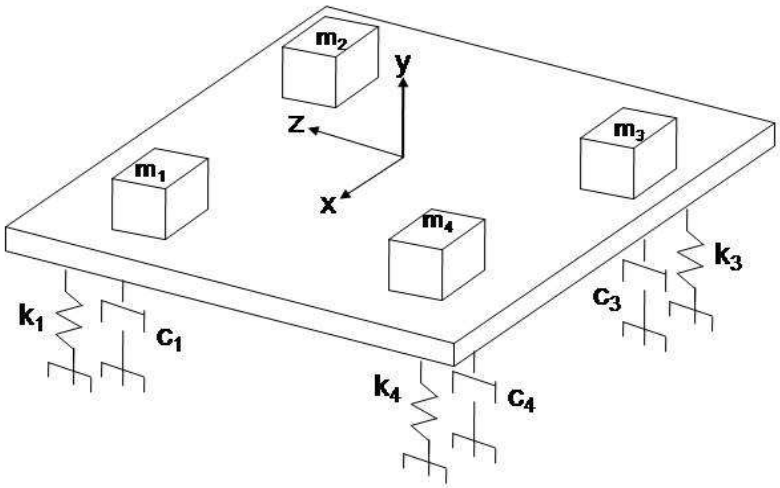

Figure 4.1: Mass, Stiffness, and Damping Coefficient Distribution

Parametric evaluation of the effect of spring stiffness, discrete mass composition and discrete mass location values were established in Tables 4.1 through 4.4. Table 4.1 shows the fixed location of the support springs while Table 4.2 presents the spring stiffnesses used. Table 4.3 presents the discrete masses used in the study, and Table 4.4 shows how the masses were distributed on the plate. A systematic notation to identify what type of vibration was considered, the value of stiffnesses used, the location of the discrete masses, and the amount of each discrete mass is given as

$$\underbrace{V}_{\textit{Vibration Type}} - \underbrace{K_I}_{\textit{Stiffness Case}} - \underbrace{M_I}_{\textit{Mass Case}} - \underbrace{L_I}_{\textit{Mass Location}}$$

where V identifies the type of vibration problem as FR for free vibration, IM for impact analysis and FF for forced vibration. For example, IM-K_1-M_2-L_3 identifies an impact analysis using equal spring stiffnesses with equal masses distributed randomly over the plate's area. In the case of no added mass, the mass location index was omitted and would append as V-K_i-M_i.

Table 4.1 Spring Coordinate Location			
Spring Number	Cartesian Coordinates		
	x (in)	y (in)	z (in)
1	17.25	-1	17.25
2	-17.25	-1	17.25
3	-17.25	-1	-17.25
4	17.25	-1	-17.25

Table 4.2 Spring Stiffnesses					
Spring Stiffness (lb/in)	Case Study				
	1	2	3	4	5
k_1	115	115	115	110	115
k_2	115	110	115	110	110
k_3	115	110	110	115	120
k_4	115	115	110	115	100

Table 4.3 Discrete Masses						
Mass (slugs)	Case Study					
	1	2	3	4	5	6
m_1	0.0	0.155	0.155	0.155	0.078	0.155
m_2	0.0	0.155	0.078	0.155	0.155	0.078
m_3	0.0	0.155	0.078	0.078	0.078	0.0
m_4	0.0	0.155	0.155	0.078	0.155	0.233

Table 4.4 Discrete Mass Location				
Location	Case Study			
	(x_1,z_1)	(x_2,z_2)	(x_3,z_3)	(x_4,z_4)
l_1	(9,9)	(12,12)	(12,12)	(9,9)
l_2	(-9,9)	(6,6)	(12,6)	(-12,12)
l_3	(-9,-9)	(12,-6)	(6,6)	(-15,-5)
l_4	(9,-9)	(6,-12)	(6,12)	(6,-6)

4.2 Free Vibration Analysis

Free vibration analysis was governed by eqns. (2.17) and (2.18). Results consisted of natural frequencies, displacement and rotation results, and target plots for various types of initial conditions. Initial conditions consisted of non-zero generalized displacements and zero generalized velocities.

Figure 4.2 shows results for displacements and rotations for FR-K_1-M_1 with an initial displacement of 0.01 ft in the x-direction only. Natural frequencies of this case were $\omega_1 = \omega_2 = 5.464$ Hz, $\omega_3 = 5.478$ Hz, $\omega_4 = 9.094$ Hz, $\omega_5 = \omega_6 = 9.104$ Hz. Modes 1 and 2 correspond to the in-plane modes, mode 3 is the transverse mode, mode 4 corresponded to the yaw mode, and modes 5 and 6 corresponded to the rotational modes. The non-zero displacement was $u_0(t)$ and the only non-zero rotation was $\theta_z(t)$. These expressions were

$$u_0(t) = 2.967\times10^{-5}\ \mathrm{Sin}[1.5708 - 57.203\,t] + 9.970\times10^{-3}\ \mathrm{Sin}[1.5708 + 34.3343\,t] \qquad (4.1)$$
$$\theta_z(t) = 6.270\times10^{-4}\ \mathrm{Sin}[1.5708 - 57.203\,t] - 6.270\times10^{-4}\ \mathrm{Sin}[1.5708 + 34.3343\,t]$$

Both motions were in-phase with each other.

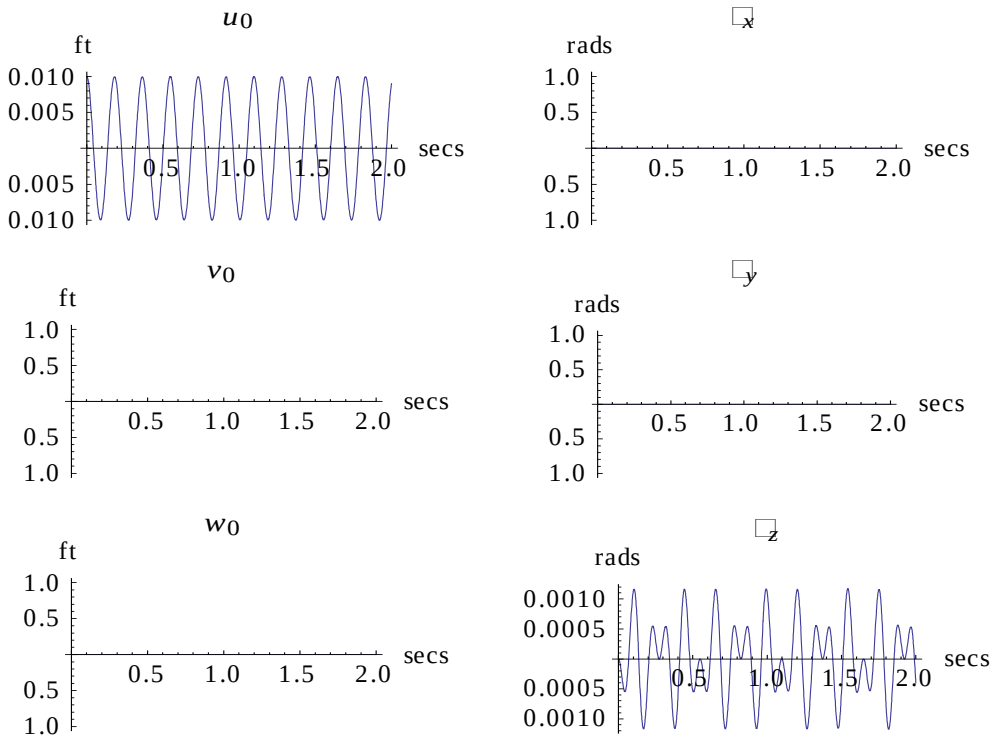

Figure 4.2 Displacement plots for free vibration equal stiffnesses, no added masses. with initial condition of $u_0(0) = 0.01$ ft.

Changing the stiffness case to case 5, or evaluating FR-K_5-M_1 for the same initial condition, highlighted the effect of unequal spring stiffness and static coupling on the motion of the platform. All displacements and angular rotations grew harmonically with the exception of $u_0(t)$. This induced motion exhibited a beating phenomena characterized by a slow variation in amplitude with rapid oscillations.

Clearly based upon spring stiffnesses, two types of motions exist. The first is identified as direct motion consistant with initial conditions and the second is indused motion based upon system properties. Another noticeable result was that the natural frequencies separated to $\omega_1 =$ 5.402 Hz, $\omega_2 =$ 5.404 Hz, $\omega_3 =$ 5.418 Hz, $\omega_4 =$ 8.804 Hz, $\omega_5 =$ 8.996 Hz, $\omega_6 =$ 9.202 Hz.

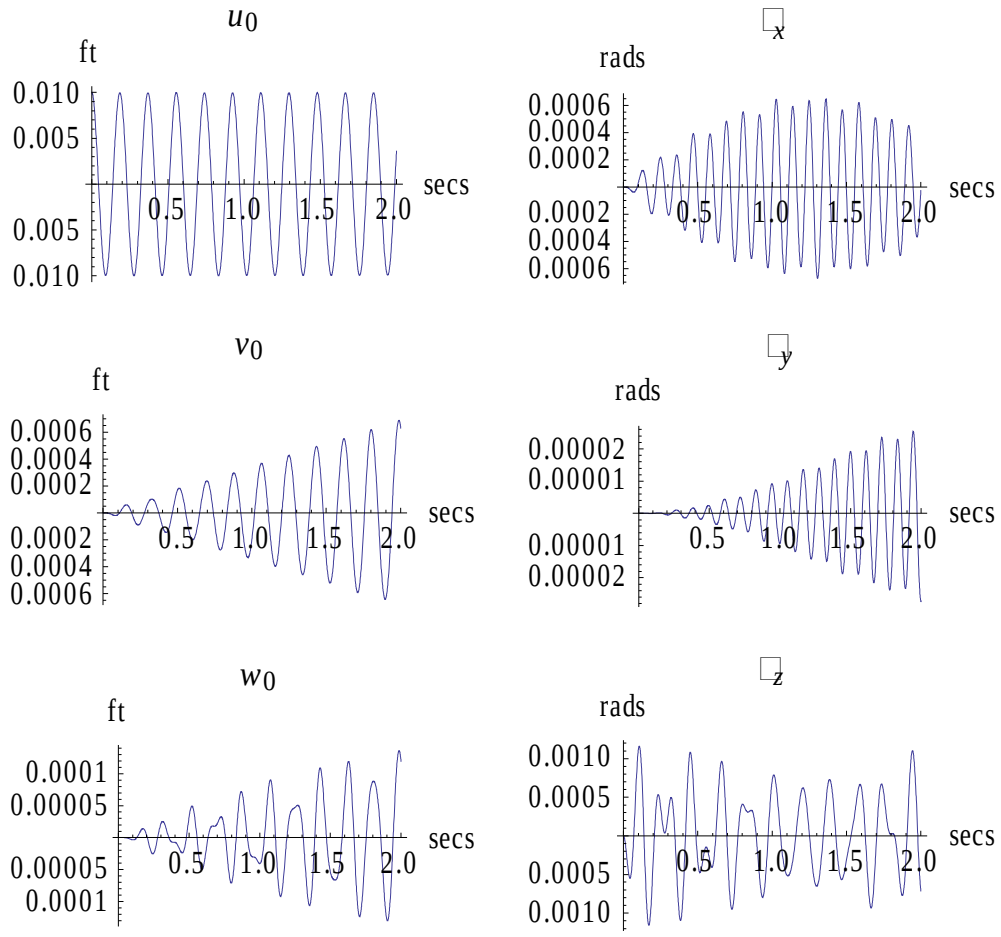

Figure 4.3 Displacement plots for free vibration unequal stiffnesses, no added masses with initial condition of $u_0(0) = 0.01$ ft.

Expressions for the displacements highlighted the coupling effects and were given as

$$
\begin{aligned}
u_0(t) &= 1.702\times10^{-5}\,\mathrm{Sin}[1.5708 - 55.3206\,t] + 1.281\times10^{-3}\,\mathrm{Sin}[1.5708 - 34.084\,t] \\
&\quad + 6.288\times10^{-3}\,\mathrm{Sin}[1.5708 + 33.9414\,t] + 2.399\times10^{-3}\,\mathrm{Sin}[1.5708 + 33.9563\,t] \\
&\quad + 3.120\times10^{-8}\,\mathrm{Sin}[1.5708 + 56.52041\,t] + 1.300\times10^{-5}\,\mathrm{Sin}[1.5708 + 57.8158\,t]
\end{aligned}
$$

$$
\begin{aligned}
v_0(t) &= -6.525\times10^{-6}\,\mathrm{Sin}[1.5708 - 55.3206\,t] + 3.342\times10^{-3}\,\mathrm{Sin}[1.5708 - 34.084\,t] \\
&\quad - 2.410\times10^{-3}\,\mathrm{Sin}[1.5708 + 33.9414\,t] - 9.199\times10^{-4}\,\mathrm{Sin}[1.5708 + 33.9563\,t] \\
&\quad - 1.196\times10^{-8}\,\mathrm{Sin}[1.5708 + 56.52041\,t] - 4.984\times10^{-6}\,\mathrm{Sin}[1.5708 + 57.8158\,t]
\end{aligned}
$$

$$
\begin{aligned}
w_0(t) &= -1.692\times10^{-5}\,\mathrm{Sin}[1.5708 - 55.3206\,t] - 4.158\times10^{-3}\,\mathrm{Sin}[1.5708 + 33.9414\,t] \\
&\quad + 4.162\times10^{-3}\,\mathrm{Sin}[1.5708 + 33.9563\,t] - 2.639\times10^{-7}\,\mathrm{Sin}[1.5708 + 56.5204\,t] \\
&\quad + 1.307\times10^{-5}\,\mathrm{Sin}[1.5708 + 57.8158\,t]
\end{aligned}
\qquad (4.3)
$$

$$
\begin{aligned}
\theta_x(t) &= 3.363\times10^{-4}\,\mathrm{Sin}[1.5708 - 55.3206\,t] - 2.940\times10^{-4}\,\mathrm{Sin}[1.5708 + 33.9414\,t] \\
&\quad + 2.508\times10^{-4}\,\mathrm{Sin}[1.5708 + 33.9563\,t] + 3.440\times10^{-8}\,\mathrm{Sin}[1.5708 + 56.204\,t] \\
&\quad - 2.931\times10^{-4}\,\mathrm{Sin}[1.5708 + 57.8158\,t]
\end{aligned}
$$

$$
\begin{aligned}
\theta_y(t) &= 8.299\times10^{-8}\,\mathrm{Sin}[1.5708 - 55.3206\,t] + 4.997\times10^{-5}\,\mathrm{Sin}[1.5708 + 33.9414\,t] \\
&\quad - 5.009\times10^{-5}\,\mathrm{Sin}[1.5708 + 33.9563\,t] - 1.441\times10^{-5}\,\mathrm{Sin}[1.5708 + 56.204\,t] \\
&\quad + 6.232\times10^{-6}\,\mathrm{Sin}[1.5708 + 57.8158\,t]
\end{aligned}
$$

$$
\begin{aligned}
\theta_z(t) &= 3.349\times10^{-4}\,\mathrm{Sin}[1.5708 - 55.3206\,t] - 4.737\times10^{-4}\,\mathrm{Sin}[1.5708 + 33.9414\,t] \\
&\quad - 1.557\times10^{-4}\,\mathrm{Sin}[1.5708 + 33.9563\,t] + 6.573\times10^{-7}\,\mathrm{Sin}[1.5708 + 56.5204\,t] \\
&\quad + 2.938\times10^{-4}\,\mathrm{Sin}[1.5708 + 57.8158\,t]
\end{aligned}
$$

Figure 4.4 shows the results for initial conditions of $u_0(0) = 0.01$ ft, $v_0(0) = -0.01$ ft and $w_0(0) = 0.01$ ft, with all other initial conditions equal to zero, since it is more difficult to prescribe angular position than displacements. Here notice that u_0 and w_0 move in-phase while θ_y and θ_z move in-phase.

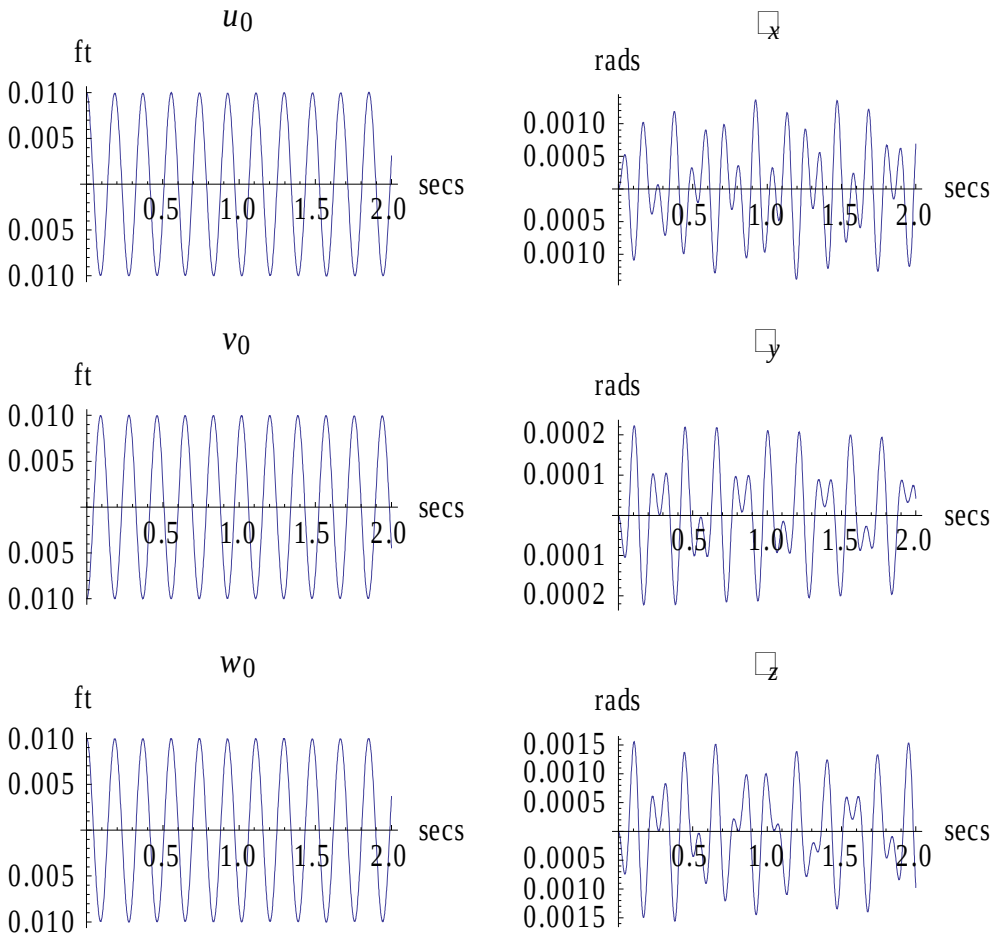

Figure 4.4 Displacement plots for free vibration unequal stiffnesses, no added masses with initial condition of $u_0(0) = 0.01$ ft, $v_0(0) = -0.01$ ft, $w_0(0) = 0.01$ ft

Below are target plots, which represent a two-dimensional projection of the motion of the platform and gave an indication of how the motions increased with distance and provided a visual perspective of the platform's motion. Here the distance was 14 ft from the center of the plate. Figure 4.5a corresponded to FR-K_1-M_1 and figure 4.5b corresponded to FR-K_5-M_1.

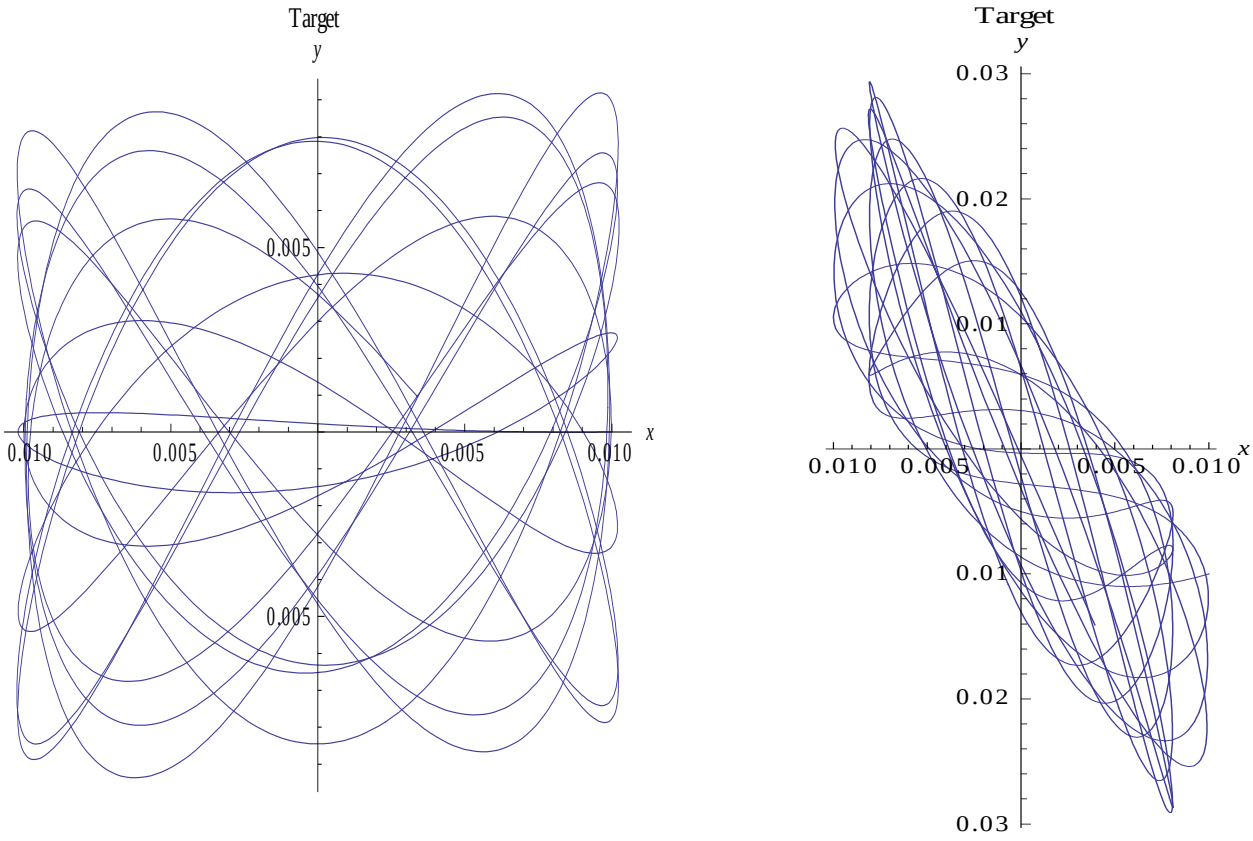

Figure 4.5 Target Plots for equal and unequal spring stiffness and no added discrete mass.

Adding mass reduced the natural frequency of the system, as well as the displacement amplitudes. Increasing the mass at points not co-located with the centroid affected rotational modes of vibration. Take, for example, the case identified as FR-K_1-M_2-L_1, which added equal discrete mass of 0.155 slugs at the center of each quadrant. The natural frequencies were $\omega_1 = \omega_2 = 5.114$Hz, $\omega_3 = 5.147$ Hz, $\omega_4 = \omega_5 = 9.104$ Hz, and $\omega_6 = 8.672$ Hz. Modes 1 and 2 corresponded to the in-plane modes, mode 3 was the transverse mode, mode 4 and 5 were the rotational modes, and mode 6 was the yaw mode. Here there was a shift in higher rotational modes. An interesting scenario was the case of unequal stiffness, with added unequal discrete

masses not arranged in a symmetric pattern about the origin, as depicted by FR-K_5-M_6-L_4. This resulted in natural frequencies that were all unique given by: $\omega_1 = 5.047$ Hz, $\omega_2 = 5.055$Hz, $\omega_3 = 5.0885$ Hz, $\omega_4 = 8.324$ Hz, $\omega_5 = 8.498$ Hz, and $\omega_6 = 8.557$ Hz. Displacement plots are shown in figure 4.5, and its target plot is presented in 4.6.

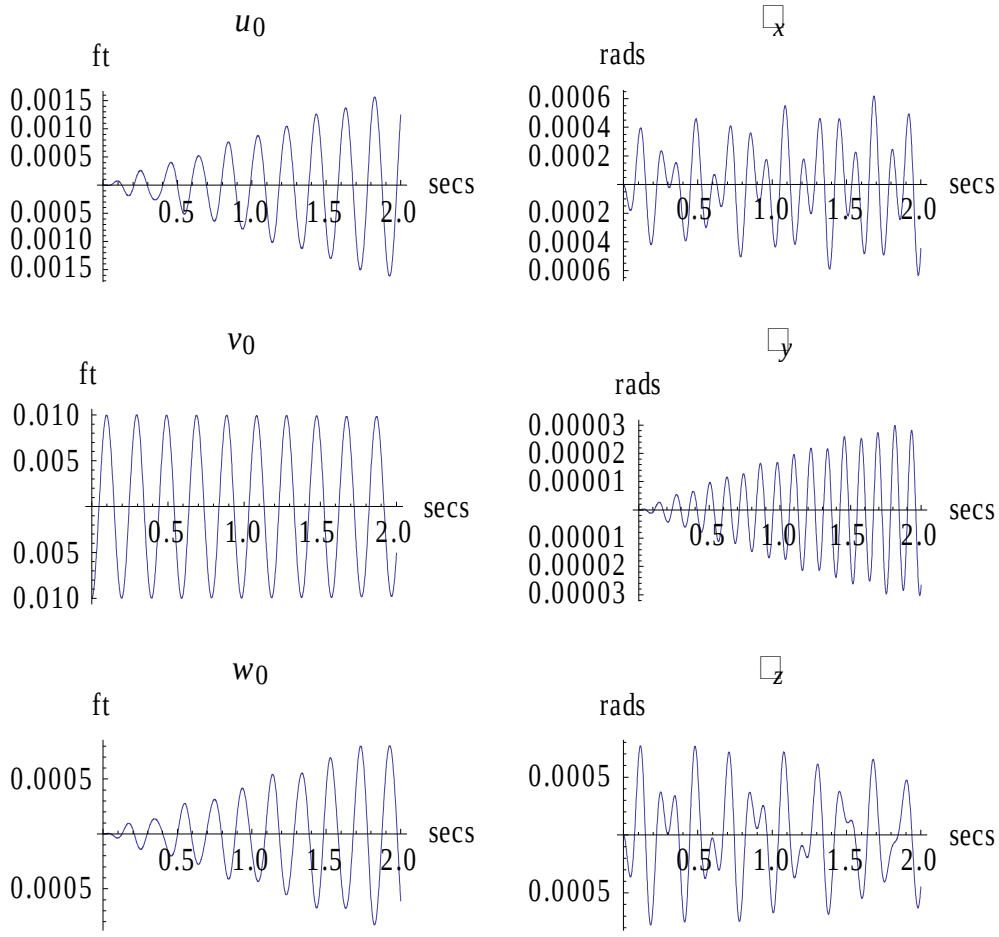

Figure 4.6 Displacement plots for free vibration unequal stiffnesses, added unequal discrete masses with initial condition of $v_0(0) = -0.01$ft

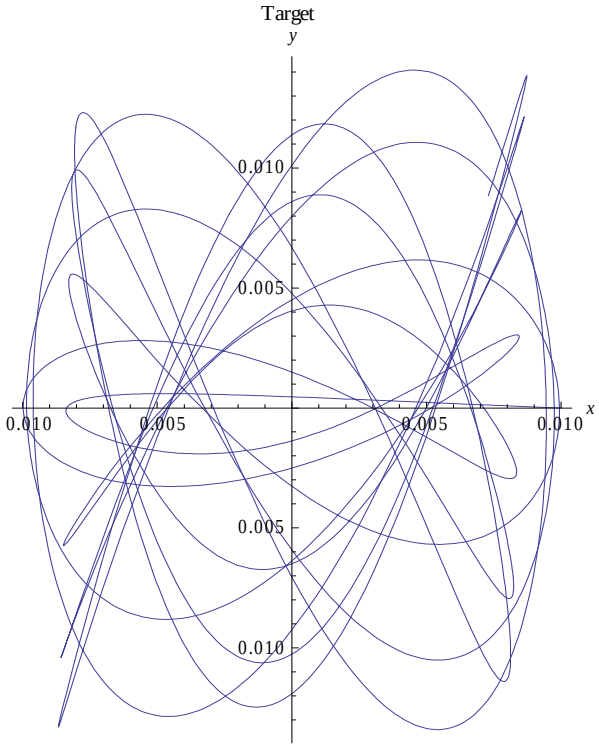

Figure 4.7 Target Plot for unequal spring stiffness and added discrete mass.

4.3 Free Vibration, Damped Analysis

In this section, damping was included in the vibration analysis and represented using a proportional damping model as presented in eqn. (3.20). Initial conditions selected were similar to those used previously. Several combinations of constants α and β were computed in order to yield realistic damping ratios. Results presented in this section followed a pattern similar to the results presented in the previous section.

Table 4.5 compares values of natural frequency ω_n, damped natural frequency ω_d, and damping ratio ζ based upon proportional damping constants α and β. Damping ratios of the order of 1 to 2 % are realistic and provide a framework for selecting proportional constants. For convenience these constants were taken to be 0.0007812 for damped free vibration, although any

set can be chosen based upon performance and design considerations. These values provided a maximum damping ratio of 2.23%.

Table 4.5 Natural Frequency, damped natural frequency and damping ratio as function of proportion constants α and β

Mode	α = 0.0125 β = 0.0125			α = 0.00625 β = 0.00625			α = 0.003125 β = 0.003125		
	ω_n	ω_d	ζ	ω_n	ω_d	ζ	ω_n	ω_d	ζ
1	5.464	4.842	0.215	5.464	5.163	0.107	5.464	5.315	0.0537
2	5.464	4.842	0.215	5.464	5.163	0.107	5.464	5.315	0.0537
3	5.478	4.853	0.215	5.478	5.176	0.108	5.478	5.329	0.0538
4	9.094	7.291	0.357	9.094	8.242	0.179	9.094	8.678	0.0893
5	9.104	7.291	0.357	9.104	8.250	0.179	9.104	8.687	0.0894
6	9.104	7.297	0.357	9.104	8.250	0.179	9.104	8.687	0.0894
Mode	α = 0.001562 β = 0.001562			α = 0.0007812 β = 0.0007812			α = 0.000390 β = 0.000390		
	ω_n	ω_d	ζ	ω_n	ω_d	ζ	ω_n	ω_d	ζ
1	5.464	5.390	0.0268	5.464	5.427	0.0134	5.464	5.446	0.0067
2	5.464	5.390	0.0268	5.464	5.427	0.0134	5.464	5.446	0.0067
3	5.478	5.404	0.0269	5.478	5.441	0.0134	5.478	5.460	0.0067
4	9.094	8.888	0.0446	9.094	8.992	0.0223	9.094	9.043	0.0111
5	9.104	8.898	0.0447	9.104	9.001	0.0223	9.104	9.053	0.0111
6	9.104	8.898	0.0447	9.104	9.001	0.0223	9.104	9.053	0.0111

The presence of damping in the vibration model resulted in a characteristic equation, which contained complex roots. The displacement expressions presented in eqn. (4.4) reflected this fact and were used to generate figure 4.8 for the case of FR-K_1-M_1. Here the plate was given an initial displacement in the x direction only. Damped natural frequencies were given as $\omega_{d1} = \omega_{d2}$ = 5.437 Hz, ω_{d3} = 5.442 Hz, ω_{d3} = 8.992 Hz, $\omega_{d5} = \omega_{d6}$ =8.708 Hz. Figure 4.9 is the target plot

and shows that the density of the plot trace became more concentrated near its origin as time increased, which reflected the effect of damping.

$$
\begin{aligned}
u_0(t) &= 2.967\times10^{-5}\ e^{-1.279\,t}\ \mathrm{Sin}[1.5934 - 56.560\,t] \\
&\quad + 9.970\times10^{-3}\ e^{-0.4608\,t}\mathrm{Sin}[1.5578 + 34.1031t] \\
\theta_z(t) &= 6.270\times10^{-4}\ e^{-1.279\,t}\ \mathrm{Sin}[1.5934 - 56.560\,t] \\
&\quad - 6.270\times10^{-4}\ e^{-0.4608\,t}\ \mathrm{Sin}[1.5578 + 34.1031\,t]
\end{aligned}
\tag{4.4}
$$

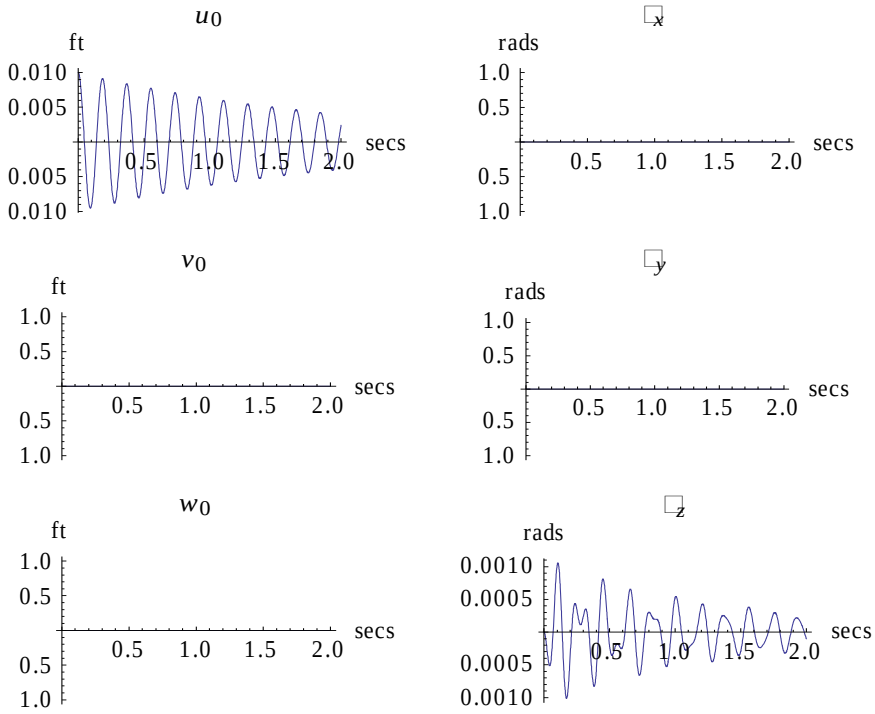

Figure 4.8 Displacement plots for free vibration unequal stiffnesses, no added masses with initial condition of $u_0(0) = 0.01$ft.

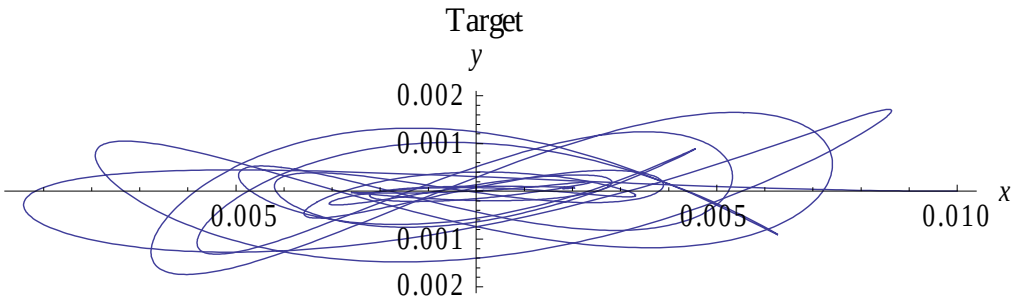

Figure 4.9 Target plot for equal stiffness, no added discrete mass damped vibration.

If the spring stiffness case changed to case 5 or FR-K_5-M_1, the solution for the six generalized displacements were given in eqns. (4.5) and (4.6). The corresponding damped natural frequencies were all distinct, with values of ω_{d1} = 5.366 Hz, ω_{d2} = 5.368 Hz, ω_{d3} = 5.382 Hz, ω_{d4} = 8.708 Hz, ω_{d5} = 8.895 Hz, ω_{d6} = 9.907 Hz.

$$
\begin{aligned}
u_0(t) = {} & 1.702\times10^{-5}\, e^{-1.196t}\, \mathrm{Sin}[1.5932-54.7195t] + 1.281\times10^{-3}\, e^{-0.453t}\, \mathrm{Sin}[1.5842-33.8211t] \\
& + 6.288\times10^{-3}\, e^{-0.4503t}\, \mathrm{Sin}[1.5574+33.7155t] + 2.399\times10^{-3}\, e^{-0.4507t}\, \mathrm{Sin}[1.5574+33.7301t] \\
& + 3.120\times10^{-8}\, e^{-1.2482t}\, \mathrm{Sin}[1.5484+55.8928t] + 1.300\times10^{-5}\, e^{-0.4507t}\, \mathrm{Sin}[1.5479+57.159t]
\end{aligned}
$$

$$
\begin{aligned}
v_0(t) = {} & -6.525\times10^{-6}\, e^{-1.196t}\, \mathrm{Sin}[1.5932-54.7195t] + 3.342\times10^{-3}\, e^{-0.453t}\, \mathrm{Sin}[1.5842-33.8211t] \\
& - 2.410\times10^{-3}\, e^{-0.4503t}\, \mathrm{Sin}[1.5574+33.7155t] - 9.199\times10^{-4}\, e^{-0.4507t}\, \mathrm{Sin}[1.5574+33.7301t] \\
& - 1.196\times10^{-8}\, e^{-1.2482t}\, \mathrm{Sin}[1.5484+55.8928t] - 4.984\times10^{-6}\, e^{-0.4507t}\, \mathrm{Sin}[1.5479+57.159t]
\end{aligned}
$$

$$
\begin{aligned}
w_0(t) = {} & -1.692\times10^{-5}\, e^{-1.196t}\, \mathrm{Sin}[1.5932-54.7195t] - 4.158\times10^{-3}\, e^{-0.453t}\, \mathrm{Sin}[1.5574+33.7155t] \\
& + 4.162\times10^{-3}\, e^{-0.4507t}\, \mathrm{Sin}[1.5574+33.7301t] - 2.639\times10^{-7}\, e^{-1.2482t}\, \mathrm{Sin}[1.5484+55.8928t] \\
& + 1.307\times10^{-5}\, e^{-0.4507t}\, \mathrm{Sin}[1.5479+57.159t]
\end{aligned}
$$

(4.5)

$$\theta_x(t) = 3.363\times10^{-4}\, e^{-1.196t}\, \mathrm{Sin}[1.5932 - 54.7195t] - 2.940\times10^{-4}\, e^{-0.453t}\, \mathrm{Sin}[1.5574 + 33.7155t] + 2.508\times10^{-4} e^{-0.4507t}\, \mathrm{Sin}[1.5574 + 33.7301t] + 3.440\times10^{-8} e^{-1.2482t}\, \mathrm{Sin}[1.5484 + 55.8928t] - 2.931\times10^{-4} e^{-0.4507t} \mathrm{Sin}[1.5479 + 57.159t]$$

$$\theta_y(t) = 8.299\times10^{-8}\, e^{-1.196t}\, \mathrm{Sin}[1.5932 - 54.7195t] + 4.997\times10^{-5}\, e^{-0.453t}\, \mathrm{Sin}[1.5574 + 33.7155t] - 5.009\times10^{-5} e^{-0.4507t}\, \mathrm{Sin}[1.5574 + 33.7301t] - 1.441\times10^{-5} e^{-1.2482t}\, \mathrm{Sin}[1.5484 + 55.8928t] + 6.232\times10^{-6} e^{-0.4507t} \mathrm{Sin}[1.5479 + 57.159t]$$

$$\theta_z(t) = 3.349\times10^{-4}\, e^{-1.196t}\, \mathrm{Sin}[1.5932 - 54.7195t] - 4.737\times10^{-4}\, e^{-0.453t}\, \mathrm{Sin}[1.5574 + 33.7155t] - 1.557\times10^{-4} e^{-0.4507t}\, \mathrm{Sin}[1.5574 + 33.7301t] + 6.573\times10^{-7} e^{-1.2482t}\, \mathrm{Sin}[1.5484 + 55.8928t] + 2.938\times10^{-4} e^{-0.4507t} \mathrm{Sin}[1.5479 + 57.159t] \quad (4.6)$$

Figure 4.10 shows the displacement as a function of time using α and $\beta = 0.0007812$. Both u_0 and v_0 were more dominant in respect to displacement magnitudes, since w_0 was on the order of 10^{-5}, while θ_y, on the order of 10^{-6}, was less significant when comparing the angular rotations.

The selection of constants α and β was based upon a desire to have a maximum damping ratio of approximately 2%. Increasing the constants raised ζ to a maximum of 4% which dampened out motions somewhat faster as shown in figure 4.12. There was a change in the damped frequencies to $\omega_{d1} = 5.037$ Hz, $\omega_{d2} = 5.3039$ Hz, $\omega_{d3} = 5.052$ Hz, $\omega_{d4} = 8.610$ Hz, $\omega_{d5} = 8.795$ Hz, and $\omega_{d6} = 8.990$ Hz.

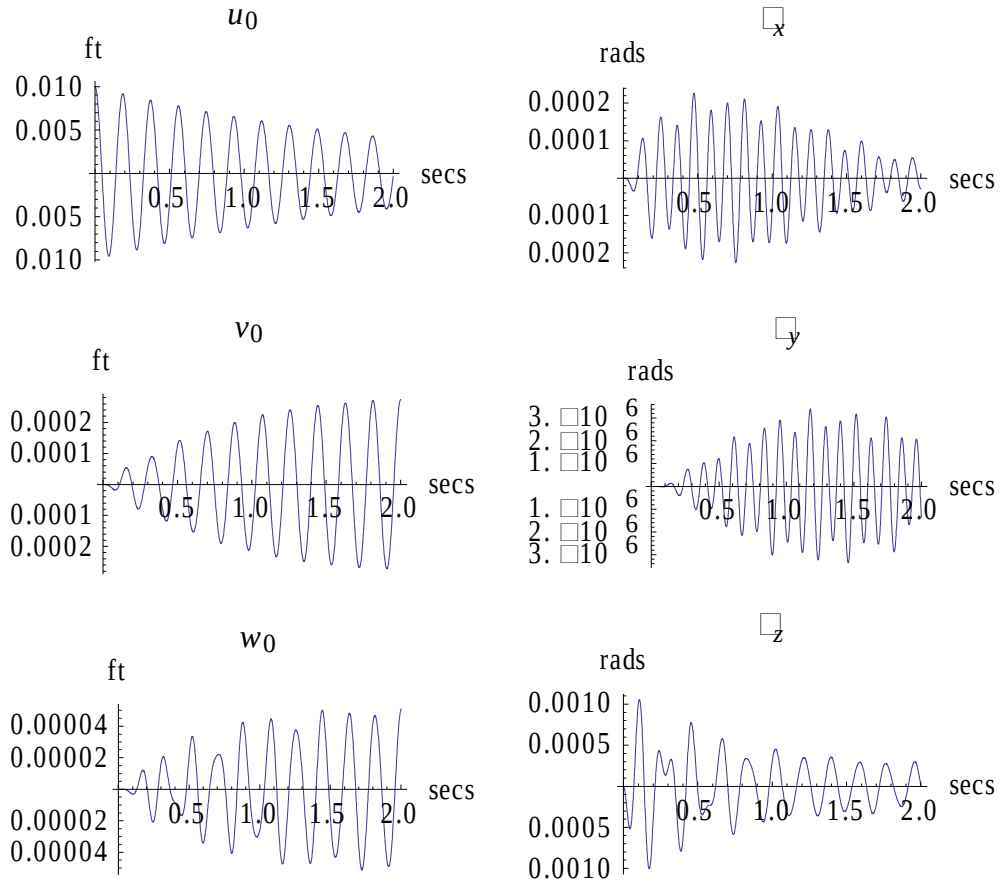

Figure 4.10. Displacement plots for free vibration, damped unequal stiffnesses, no added discrete masses with initial condition of $u_0(0) = 0.01$ft with $\alpha = 0.0007812$, $\beta = 0.0007812$

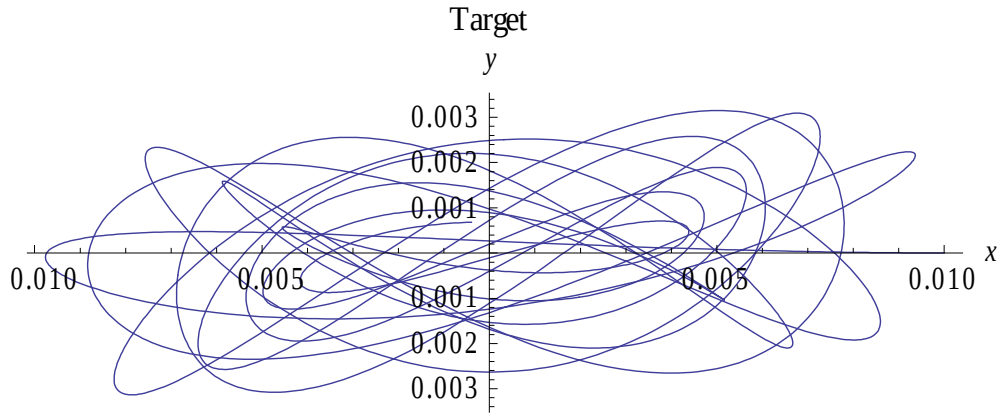

Figure 4.11 Target Plot for unequal spring stiffness and no added discrete mass (damped vibration).

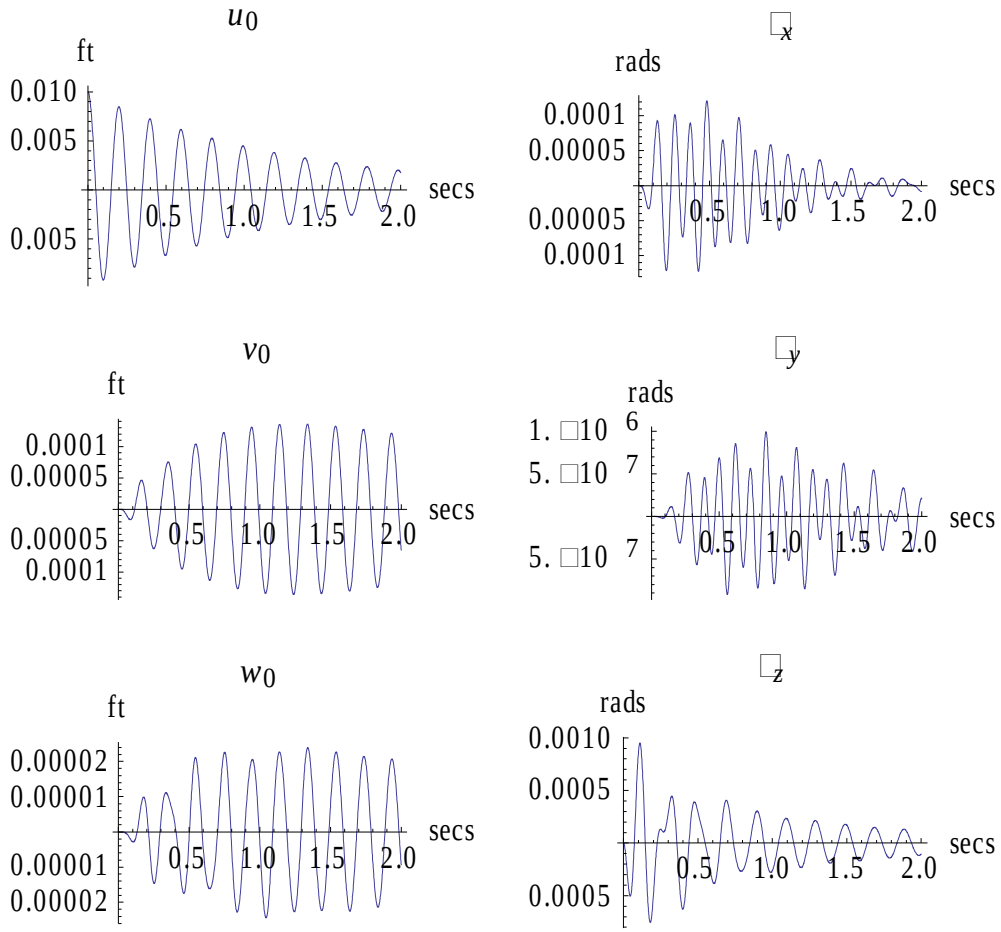

Figure 4.12 Displacement plots for free vibration unequal stiffnesses, added discrete masses with initial condition of $u_0(0) = 0.01$ft with $\alpha = 0.001562$, $\beta = 0.001562$

CHAPTER 5
IMPACT ANALYSIS

5.1 Introduction

Before moving onto forced vibration, some results are presented for impact analysis. Impact analysis had the same governing differential equations as free vibration, but here velocity and angular velocity initial conditions were prescribed instead of displacements and angular rotations. These conditions corresponded to a change in both linear and angular momentum due to impulsive forces and moments, expressed in eqn. (2.19). The impact response depended upon impact location and mass of the impacting hammer. Generalized displacement results are presented for several impact points on the plate using and impacting hammer of about 10 lb. These results were generated for a plate with unequal spring stiffnesses, discrete masses arranged arbitrarily, and damping, which is case IM-K_5-M_6-L_4

To evaluate the initial conditions required the duration of the impact event and its intensity. For a constant impact force, eqn. (2.19) evaluates to

$$v(0^+) = \frac{F_{ave}\Delta t}{m}$$

$$\dot{\theta}_x(0^+) = \frac{M_{xx}\Delta t}{I_{xx}} \qquad (5.1)$$

$$\dot{\theta}_z(0^+) = \frac{M_{zz}\Delta t}{I_{zz}}$$

where F_{ave} is the average impact force intensity, and Δt is the time of the impact. For this analysis the impact intensity of 10 lb for a duration of 0.02 secs was used. Impact analysis does not necessary start at time t = 0 secs. With the use of the kronecker delta function δ, this delay was readily incorporated. Table 5.1 provided locations where the impact would take place. These locations were not unique and represented any number of combinations of coordinates

where an impact could take place. Impact locations along the z-axis produced target plots that were essentially vertical. The nomenclature introduced in chapter three for tracking vibration cases is augmented here to track impact location. The new notation introduces P_i. P_1 in the case IM-K_5-M_6-L_4-P_1 specifies the impact point to correspond to that presented in table 5.1. All parameters presented for damped analysis are maintained here.

Table 5.1 Impact Location Placement

Location	(x_1,z_1)
P_1	(0,0)
P_2	(18,0)
P_3	(-18,0)

The case considered for impact analysis was IM-K_5-M_6-L_4-P_i. The initial conditions were $v_0(0^+)$ = -0.0382848 ft/s, $\theta_x(0^+)$ = 0.0 rad/s and $\theta_z(0^+)$ = 0.0753376 rad/s. The solution of eqn.(2.17) was

$$
\begin{aligned}
u_0(t) = (&7.6899 \times 10^{-7}\, e^{-1.13048\,(-0.5+t)}\, \mathrm{Sin}[53.220\,4\,(-0.5+t)] \\
&+ 2.4318 \times 10^{-4}\, e^{-0.39845\,(-0.5+t)}\, \mathrm{Sin}[31.723\,5\,(-0.5+t)] \\
&+ 7.6868 \times 10^{-5}\, e^{-0.399138\,(-0.5+t)}\, \mathrm{Sin}[31.750\,7\,(-0.5+t)] \\
&+ 1.6105 \times 10^{-6}\, e^{-1.09309\,(-0.5+t)}\, \mathrm{Sin}[52.341\,9\,(-0.5+t)] \\
&+ 8.2506 \times 10^{-8}\, e^{-1.12574\,(-0.5+t)}\, \mathrm{Sin}[53.109\,8\,(-0.5+t)])\,\delta(t-0.5)
\end{aligned}
$$

$$
\begin{aligned}
v_0(t) = (&-9.3065 \times 10^{-8}\, e^{-1.13048\,(-0.5+t)}\, \mathrm{Sin}[53.220\,4\,(-0.5+t)] \\
&- 8.4358 \times 10^{-5}\, e^{-0.39845\,(-0.5+t)}\, \mathrm{Sin}[31.723\,5\,(-0.5+t)] \\
&- 1.5038 \times 10^{-5}\, e^{-0.399138\,(-0.5+t)}\, \mathrm{Sin}[31.750\,7\,(-0.5+t)] \\
&- 5.5969 \times 10^{-7}\, e^{-1.09309\,(-0.5+t)}\, \mathrm{Sin}[52.341\,9\,(-0.5+t)] \\
&- 2.8323 \times 10^{-9}\, e^{-1.12574\,(-0.5+t)}\, \mathrm{Sin}[53.109\,8\,(-0.5+t)])\,\delta(t-0.5)
\end{aligned}
\qquad (5.2)
$$

$$
\begin{aligned}
w_0(t) = (&6.8405 \times 10^{-7}\, e^{-1.13048\,(-0.5+t)}\, \mathrm{Sin}[53.220\,4\,(-0.5+t)] \\
&- 1.8476 \times 10^{-4}\, e^{-0.39845\,(-0.5+t)}\, \mathrm{Sin}[31.723\,5\,(-0.5+t)] \\
&+ 1.0800 \times 10^{-4}\, e^{-0.399138\,(-0.5+t)}\, \mathrm{Sin}[31.750\,7\,(-0.5+t)] \\
&- 1.5808 \times 10^{-6}\, e^{-1.09309\,(-0.5+t)}\, \mathrm{Sin}[52.341\,9\,(-0.5+t)] \\
&+ 1.3300 \times 10^{-7}\, e^{-1.12574\,(-0.5+t)}\, \mathrm{Sin}[53.109\,8\,(-0.5+t)])\,\delta(t-0.5)
\end{aligned}
$$

$$\theta_x(t) = (-6.4761\times 10^{-6}\, e^{-1.13048\,(-0.5+t)}\, \mathrm{Sin}[53.220\ 4\,(-0.5+t)]$$
$$-1.9894\times 10^{-5}\, e^{-0.39845\,(-0.5+t)}\, \mathrm{Sin}[31.723\ 5\,(-0.5+t)]$$
$$+9.9589\times 10^{-6}\ e^{-0.399138\,(-0.5+t)}\, \mathrm{Sin}[31.750\ 7\,(-0.5+t)]$$
$$+1.3363\times 10^{-5}\, e^{-1.09309\,(-0.5+t)}\, \mathrm{Sin}[52.341\ 9\,(-0.5+t)]$$
$$-7.511\times 10^{-7}\, e^{-1.12574\,(-0.5+t)}\, \mathrm{Sin}[53.109\ 8\,(-0.5+t)])\,\delta(t-0.5)$$

$$\theta_y(t) = (-2.6473\times 10^{-6}\, e^{-1.13048\,(-0.5+t)}\, \mathrm{Sin}[53.220\ 4\,(-0.5+t)]$$
$$+1.7463\times 10^{-6}\, e^{-0.39845\,(-0.5+t)}\, \mathrm{Sin}[31.723\ 5\,(-0.5+t)]$$
$$-1.7869\times 10^{-6}\ e^{-0.399138\,(-0.5+t)}\, \mathrm{Sin}[31.750\ 7\,(-0.5+t)]$$
$$+1.0051\times 10^{-6}\, e^{-1.09309\,(-0.5+t)}\, \mathrm{Sin}[52.341\ 9\,(-0.5+t)]$$
$$+1.6874\times 10^{-6}\, e^{-1.12574\,(-0.5+t)}\, \mathrm{Sin}[53.109\ 8\,(-0.5+t)])\,\delta(t-0.5) \qquad (5.3)$$

$$\theta_z(t) = (6.9201\times 10^{-6}\, e^{-1.13048\,(-0.5+t)}\, \mathrm{Sin}[53.220\ 4\,(-0.5+t)]$$
$$-2.6982\times 10^{-5}\, e^{-0.39845\,(-0.5+t)}\, \mathrm{Sin}[31.723\ 5\,(-0.5+t)]$$
$$-7.3369\times 10^{-6}\ e^{-0.399138\,(-0.5+t)}\, \mathrm{Sin}[31.750\ 7\,(-0.5+t)]$$
$$+1.3258\times 10^{-5}\, e^{-1.09309\,(-0.5+t)}\, \mathrm{Sin}[52.341\ 9\,(-0.5+t)]$$
$$+5.0184\times 10^{-7}\, e^{-1.12574\,(-0.5+t)}\, \mathrm{Sin}[53.109\ 8\,(-0.5+t)])\,\delta(t-0.5)$$

with the natural frequencies of ω_{n1} = 5.0807 Hz, ω_{n2} = 5.0851 Hz, ω_{n3} = 5.1117 Hz, ω_{n4} = 8.4179 Hz, ω_{n5} = 8.5427 Hz, ω_{n6} = 8.5607 Hz, and the damped natural frequencies of ω_{d1} = 5.0489 Hz, ω_{d2} = 5.0532 Hz, ω_{d3} = 5.0847 Hz, ω_{d4} = 8.3304 Hz, ω_{d5} = 8.4526 Hz, and ω_{d6} = 8.4702 Hz. Figure 5.1 presents plots of displacement vs. time. In these graphs, displacements v_0 and w_0 moved in-phase while angular rotations θ_x and θ_z motions were in-phase with the magnitude of θ_y. However, θ_y was two orders of magnitude smaller than either θ_x or θ_z. Figure 5.2 provides the target plot for this case showing the effect of angular rotations θ_x and θ_z on this traced displacement. Figure 5.3 and 5.4 and figures 5.5 and 5.6 are displacement-target plot sets for impact locations at P_2 and P_3, respectively.

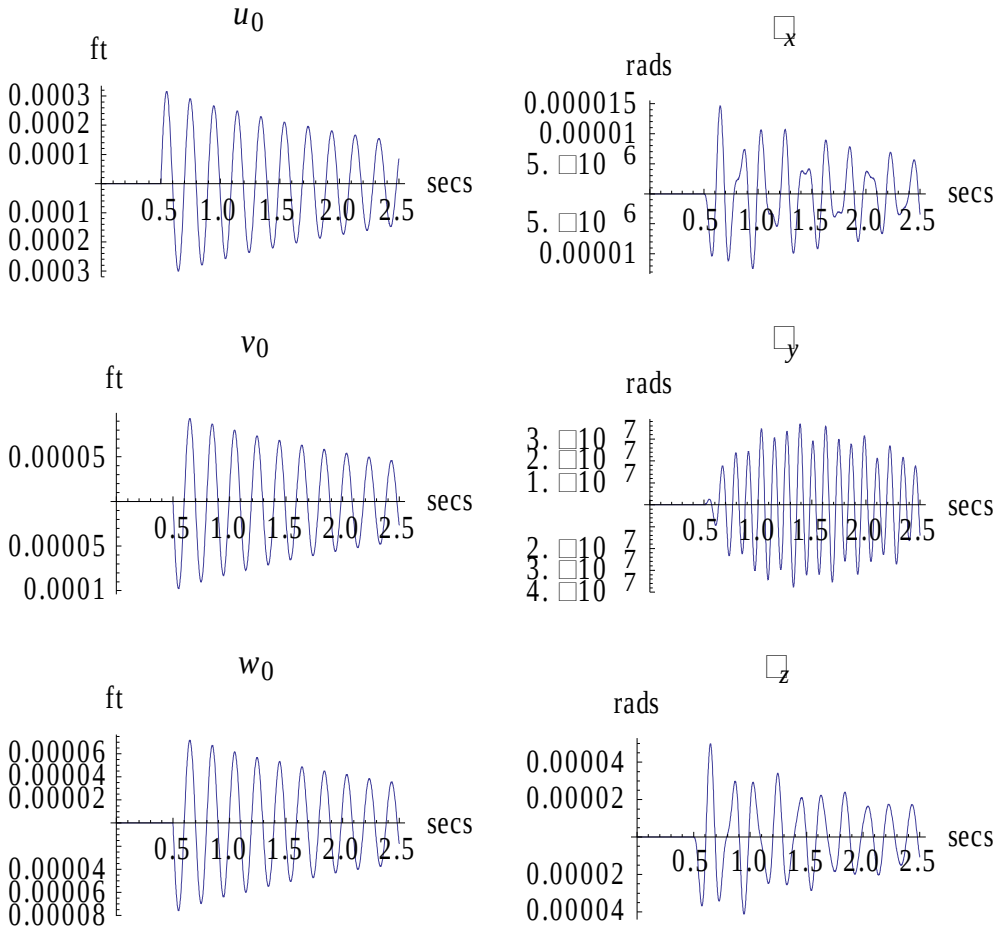

Figure 5.1 Displacement plots for impact unequal stiffnesses, added discrete with α = 0.001562, β = 0.001562

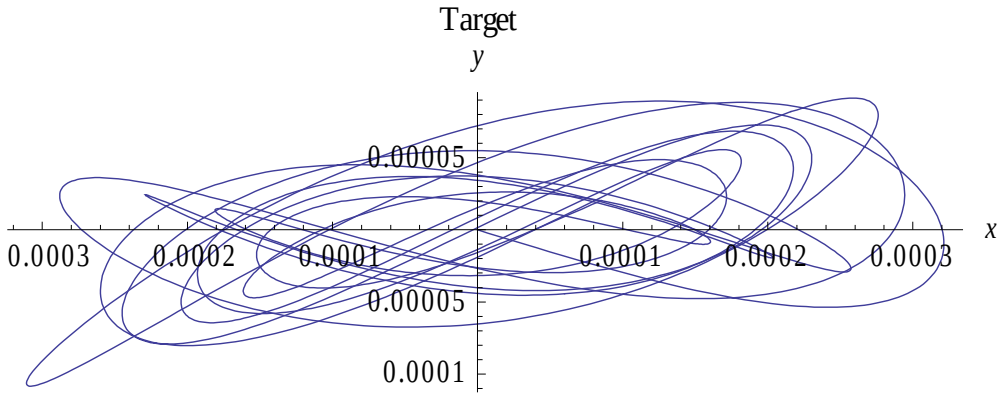

Figure 5.2 Target plot for impact analysis with impact located at the origin.

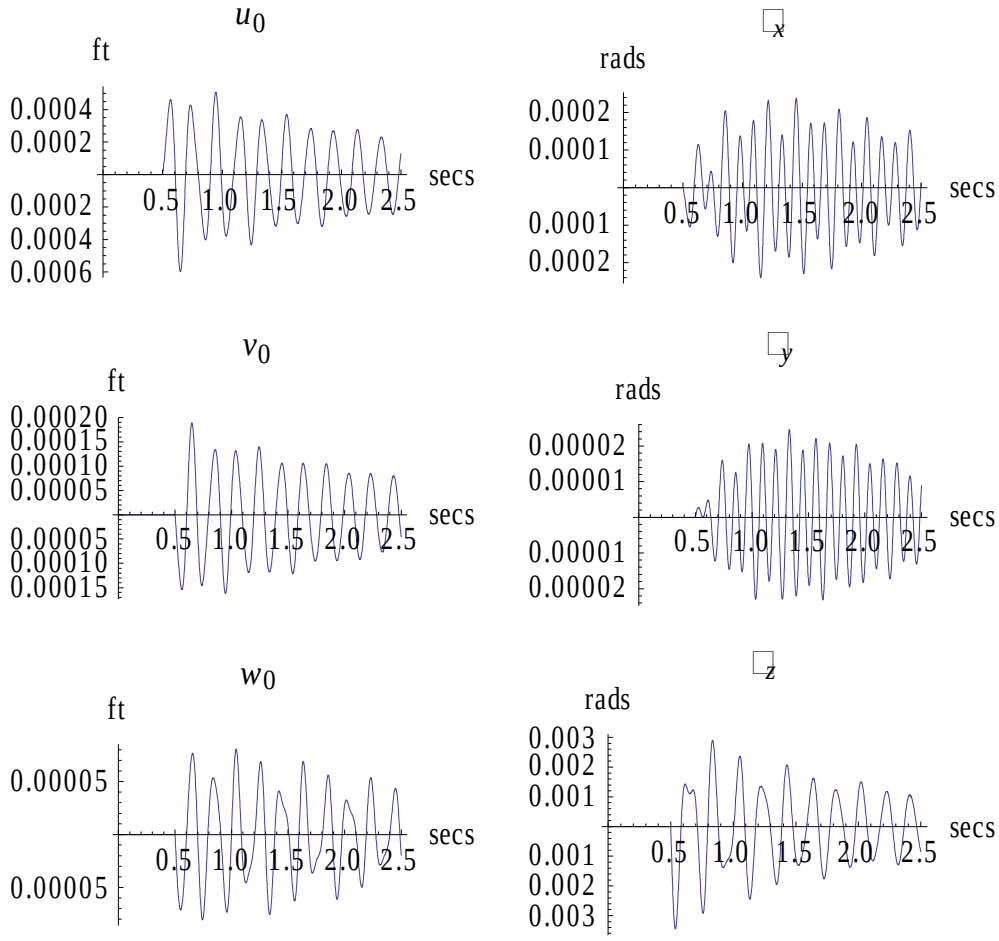

Figure 5.3 Displacement plots for impact at location P_2

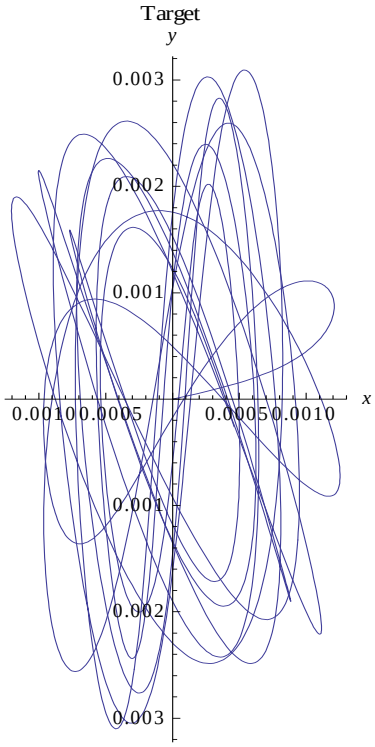

Figure 5.4 Target plot for impact at location P_2

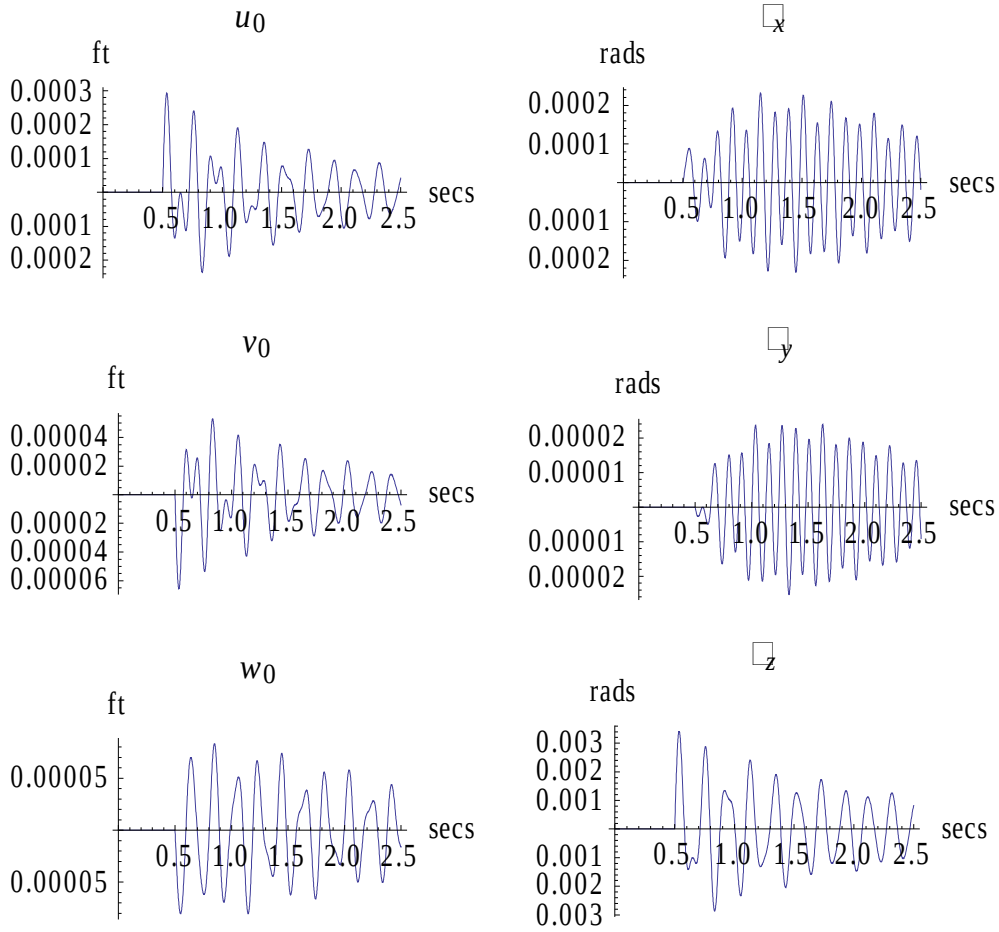

Figure 5.5 Displacement plots for impact at location P_3

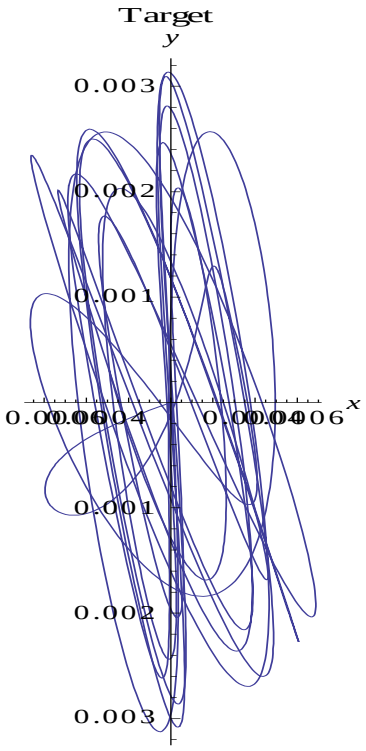

Figure 5.6 Target plot for impact at location P_3

CHAPTER 6

FORCED VIBRATION

6.1 Introduction

In this chapter, forced vibration analysis of the platform system is presented. Unlike previous results, the forcing function was constantly applied to the system, which produced both a transient and steady state solution. Also unlike the previous discussions, the governing equations of motion included representations of the forcing functions, depicted as inertial actuators. This inclusion expanded the system of governing equations from six degrees to as many as ten degrees of freedom. The equations of motion were solved for the steady-state solutions since previous results captured transient results.

Two inertial actuators are typical for the optical platform, and each is modeled as a second order system. These actuators were placed and oriented in such a way to generate in-plane displacement u_0, transverse displacement v_0, and all three angular rotations. The forcing function was represented as a single harmonic function such as $F_1(t) = F_1 Sin(\omega_1 t)$ or a linear combination of multiple harmonic functions such as

$F(t) = F_1 Sin(\omega_1\ t) + F_2 Sin(\omega_2\ t) + F_2 Sin(\omega_2\ t)$. Both cases were considered here. Since the problem was linear in nature, displacement solutions for the case of multiple frequency forcing function were obtained through a superposition of the displacement solution at each forcing frequency. Results presented here considered the case of unequal stiffenesses with added discrete masses arbitrarily located on the plate.

Refer to chapter 4 on free vibration for an explanation of the systematic notation used within this chapter to identify which stiffness, mass composition, and mass location cases are used in each study. These variables follow the pattern outlined in tables 4.1 through 4.4.

6.2 Forced Vibration Analysis

Forced vibration of the platform used two actuators whose forcing functions were given by

$$F_1(t) = 10\ Sin(75t)$$
$$F_2(t) = 10\ Sin(25t) \qquad (6.1)$$

Forcing function $F_1(t)$ was oriented 45˚ relative to the horizontal, and $F_2(t)$ was oriented in the vertical position only. The equations that governed steady-state forced vibration were given by (2.17). These equations are shown in complete detail in Appendix A-1. A modal solution approach was used to decouple the problem, solve it in modal coordinates, and transform it back to the original coordinate system to obtain the solution of the original problem. The system investigated was FF-K_5-M_6-L_4. The constants α and β used for the damping ratio were 0.0007812. With forcing functions given by eqn. (6.1) and system properties given, the steady state solutions consisted of natural frequencies of ω_{n1} = 4.9414 Hz, ω_{n2} = 6.4366 Hz, ω_{n3} = 7.2966 Hz, ω_{n4} = 8.5514 Hz, ω_{n5} = 8.6176 Hz, ω_{n6} = 9.2568 Hz and damped natural of ω_{d1} = 4.9114 Hz, ω_{d2} = 6.3855 Hz, ω_{d3} = 7.2310, ω_{d4} = 8.4612 Hz, ω_{d5} = 8.5259 Hz, ω_{d6} = 9.1511 Hz. The displacement equations became

$$u_0(t) = 1.00406\times10^{-6}\,\mathrm{Sin}[0.0121293 -75\,t] - 0.000321209\,\mathrm{Sin}[0.0240309 -75\,t]$$
$$+1.31285\times10^{-6}\,\mathrm{Sin}[0.0349573 -75\,t]-5.42389\times10^{-7}\,\mathrm{Sin}[0.0617196 -75\,t]$$
$$-9.55247\times10^{-6}\,\mathrm{Sin}[0.0637154 -75\,t]+5.38026\times10^{-6}\,\mathrm{Sin}[0.0881979 -75\,t]$$
$$+4.3727\times10^{-6}\,\mathrm{Sin}[0.0198073 +25\,t]-5.81755\times10^{-7}\,\mathrm{Sin}[0.0198115 +25\,t] \qquad (6.2)$$
$$-5.26029\times10^{-6}\,\mathrm{Sin}[0.0198166 +25\,t]-1.62503\times10^{-7}\,\mathrm{Sin}[0.0239584 +25\,t]$$
$$-0.0000139863\,\mathrm{Sin}[0.0248248 +25\,t]-2.58145\times10^{-6}\,\mathrm{Sin}[0.0249298 +25\,t]$$
$$+6.37135\times10^{-7}\,\mathrm{Sin}[0.0278009 +25\,t]+0.0000994562\,\mathrm{Sin}[0.0316172 +25\,t]$$
$$-0.0000191568\,\mathrm{Sin}[0.0555397 +25\,t]+2.53003\times10^{-6}\,\mathrm{Sin}[0.0670112 +75\,t]$$
$$-0.0000395334\,\mathrm{Sin}[0.0671549 +75\,t]+3.24891\times10^{-6}\,\mathrm{Sin}[0.0673307 +75\,t]$$

$$v_0(t) = 0.000279697\,\mathrm{Sin}[0.0121293 -75\,t]+1.00761\times10^{-6}\,\mathrm{Sin}[0.0240309 -75\,t]$$
$$-1.94145\times10^{-6}\,\mathrm{Sin}[0.0349573 -75\,t]-2.69454\times10^{-7}\,\mathrm{Sin}[0.0617196 -75\,t]$$
$$-8.67708\times10^{-7}\,\mathrm{Sin}[0.0637154 -75\,t]-8.28308\times10^{-6}\,\mathrm{Sin}[0.0881979 -75\,t]$$
$$+0.0000409697\,\mathrm{Sin}[0.0198073 +25\,t]+1.43775\times10^{-7}\,\mathrm{Sin}[0.0198115 +25\,t] \qquad (6.3)$$
$$+5.30289\times10^{-7}\,\mathrm{Sin}[0.0198166 +25\,t]+2.50179\times10^{-7}\,\mathrm{Sin}[0.0239584 +25\,t]$$
$$-1.27046\times10^{-6}\,\mathrm{Sin}[0.0248248 +25\,t]-1.28244\times10^{-6}\,\mathrm{Sin}[0.0249298 +25\,t]$$
$$-9.42197\times10^{-7}\,\mathrm{Sin}[0.0278009 +25\,t]-3.11986\times10^{-7}\,\mathrm{Sin}[0.0316172 +25\,t]$$
$$-0.00533642\,\mathrm{Sin}[0.0555397 +25\,t]+0.0000237049\,\mathrm{Sin}[0.0670112 +75\,t]$$
$$+9.77027\times10^{-6}\,\mathrm{Sin}[0.0671549 +75\,t]-3.27522\times10^{-7}\,\mathrm{Sin}[0.0673307 +75\,t]$$

$$w_0(t)=-1.44417\times10^{-6}\,\mathrm{Sin}[0.0121293-75\,t]-1.82636\times10^{-6}\,\mathrm{Sin}[0.0240309-75\,t]$$
$$-0.0000923278\,\mathrm{Sin}[0.0349573-75\,t]-2.91666\times10^{-7}\,\mathrm{Sin}[0.0617196-75\,t]$$
$$+0.0000194523\,\mathrm{Sin}[0.0637154-75\,t]+0.000115661\,\mathrm{Sin}[0.0881979-75\,t]$$
$$-4.19896\times10^{-7}\,\mathrm{Sin}[0.0198073+25\,t]-2.37918\times10^{-9}\,\mathrm{Sin}[0.0198115+25\,t]$$
$$+5.15085\times10^{-7}\,\mathrm{Sin}[0.0198166+25\,t]-3.49338\times10^{-6}\,\mathrm{Sin}[0.0239584+25\,t] \qquad (6.4)$$
$$+0.000028481\,\mathrm{Sin}[0.0248248+25\,t]-1.38816\times10^{-6}\,\mathrm{Sin}[0.0249298+25\,t]$$
$$-0.0000448072\,\mathrm{Sin}[0.0278009+25\,t]+5.65496\times10^{-7}\,\mathrm{Sin}[0.0316172+25t]$$
$$+0.0000275536\,\mathrm{Sin}[0.0555397+25\,t]-2.4295\times10^{-7}\,\mathrm{Sin}[0.0670112+75\,t]$$
$$-1.61678\times10^{-7}\,\mathrm{Sin}[0.0671549+75\,t]-3.18132\times10^{-7}\,\mathrm{Sin}[0.0673307+75\,t]$$

$$\theta_x(t)=4.60572\times10^{-6}\,\mathrm{Sin}[0.0121293-75\,t]-2.07747\times10^{-6}\,\mathrm{Sin}[0.0240309-75\,t]$$
$$+0.0000448641\,\mathrm{Sin}[0.0349573-75\,t]+7.71136\times10^{-6}\,\mathrm{Sin}[0.0617196-75\,t]$$
$$+8.16241\times10^{-6}\,\mathrm{Sin}[0.0637154-75\,t]+0.000256036\,\mathrm{Sin}[0.0881979-75\,t]$$
$$+0.0000109739\,\mathrm{Sin}[0.0198073+25\,t]+8.90035\times10^{-8}\,\mathrm{Sin}[0.0198115+25\,t] \qquad (6.5)$$
$$-0.000013611\,\mathrm{Sin}[0.0198166+25\,t]-7.7332\times10^{-6}\,\mathrm{Sin}[0.0239584+25\,t]$$
$$+0.000011951\,\mathrm{Sin}[0.0248248+25\,t]+0.0000367015\,\mathrm{Sin}[0.0249298+25t]$$
$$+0.0000217728\,\mathrm{Sin}[0.0278009+25\,t]+6.43246\times10^{-7}\,\mathrm{Sin}[0.0316172+25\,t]$$
$$-0.0000878739\,\mathrm{Sin}[0.0555397+25\,t]+6.34946\times10^{-6}\,\mathrm{Sin}[0.0670112+75\,t]$$
$$+6.04827\times10^{-6}\,\mathrm{Sin}[0.0671549+75\,t]+8.40657\times10^{-6}\,\mathrm{Sin}[0.0673307+75\,t]$$

$$\theta_y(t)=-2.82214\times10^{-8}\ \mathrm{Sin}[0.0121293 -75\ t]+6.7708\times10^{-6}\ \mathrm{Sin}[0.0240309 -75\ t]$$
$$+0.0000196566\ \mathrm{Sin}[0.0349573 -75\ t]-8.9916\times10^{-6}\ \mathrm{Sin}[0.0617196 -75\ t]$$
$$+0.0000263297\ \mathrm{Sin}[0.0637154 -75\ t]+0.000111047\ \mathrm{Sin}[0.0881979 -75\ t]$$
$$-1.41948\times10^{-6}\ \mathrm{Sin}[0.0198073 +25\ t]+1.76317\times10^{-7}\ \mathrm{Sin}[0.0198115 +25\ t]$$
$$+1.40466\times10^{-6}\ \mathrm{Sin}[0.0198166 +25\ t]-3.35401\times10^{-6}\ \mathrm{Sin}[0.0239584 +25\ t] \quad (6.6)$$
$$+0.0000385506\ \mathrm{Sin}[0.0248248 +25\ t]-0.0000427947\ \mathrm{Sin}[0.0249298 +25\ t]$$
$$+9.53946\times10^{-6}\ \mathrm{Sin}[0.0278009 +25\ t]-2.09645\times10^{-6}\ \mathrm{Sin}[0.0316172 +25\ t]$$
$$+5.38444\times10^{-7}\ \mathrm{Sin}[0.0555397 +25\ t]-8.21303\times10^{-7}\ \mathrm{Sin}[0.0670112 +75\ t]$$
$$+0.0000119817\ \mathrm{Sin}[0.0671549 +75\ t]-8.67559\times10^{-7}\ \mathrm{Sin}[0.0673307 +75\ t]$$

$$\theta_z(t)= 4.69373\times10^{-6}\ \mathrm{Sin}[0.0121293 -75\ t]-0.0000375903\ \mathrm{Sin}[0.0240309 -75\ t]$$
$$+4.25126\times10^{-6}\ \mathrm{Sin}[0.0349573 -75\ t]+1.42329\times10^{-6}\ \mathrm{Sin}[0.0617196 -75\ t]$$
$$+0.000331645\ \mathrm{Sin}[0.0637154 -75\ t]-0.0000274044\ \mathrm{Sin}[0.0881979 -75\ t]$$
$$-0.0000150431\ \mathrm{Sin}[0.0198073 +25\ t]+3.08941\times10^{-7}\ \mathrm{Sin}[0.0198115 +25\ t]$$
$$-0.0000113176\ \mathrm{Sin}[0.0198166 +25\ t]+8.27713\times10^{-7}\ \mathrm{Sin}[0.0239584 +25\ t] \quad (6.7)$$
$$+0.000485579\ \mathrm{Sin}[0.0248248 +25\ t]+6.77404\times10^{-6}\ \mathrm{Sin}[0.0249298 +25\ t]$$
$$+2.06316\times10^{-6}\ \mathrm{Sin}[0.0278009 +25\ t]+0.0000116391\ \mathrm{Sin}[0.0316172 +25\ t]$$
$$-0.000089553\ \mathrm{Sin}[0.0555397 +25\ t]-8.70387\times10^{-6}\ \mathrm{Sin}[0.0670112 +75\ t]$$
$$+0.0000209942\ \mathrm{Sin}[0.0671549 +75\ t]+6.9901\times10^{-6}\ \mathrm{Sin}[0.0673307 +75\ t]$$

Although long and tedious, the solutions contained no more than seven combinations of the Sine function at each frequency and a phase angle. These equations were plotted in figure 6.1. Most notable was the slowing period of oscillation in displacement $v_0(t)$ and rapid oscillation in $\theta_z(t)$.

Figure 6.2 shows the same input information with the exception that the frequencies were exchanged. With these changes it was possible to assess the effect of the actuator orientation on the motion of the platform. By comparing Figures 6.1 and 6.2 it was seen that the actuator oriented at 45˚ dominates the motion when forcing amplitudes were equal. Figure 6.3 shows the displacement results using same frequency of 25 rad/s. In-plane displacement w_0 was relatively small when compared to the other two components. Also, rotations θ_x and θ_y were in-phase.

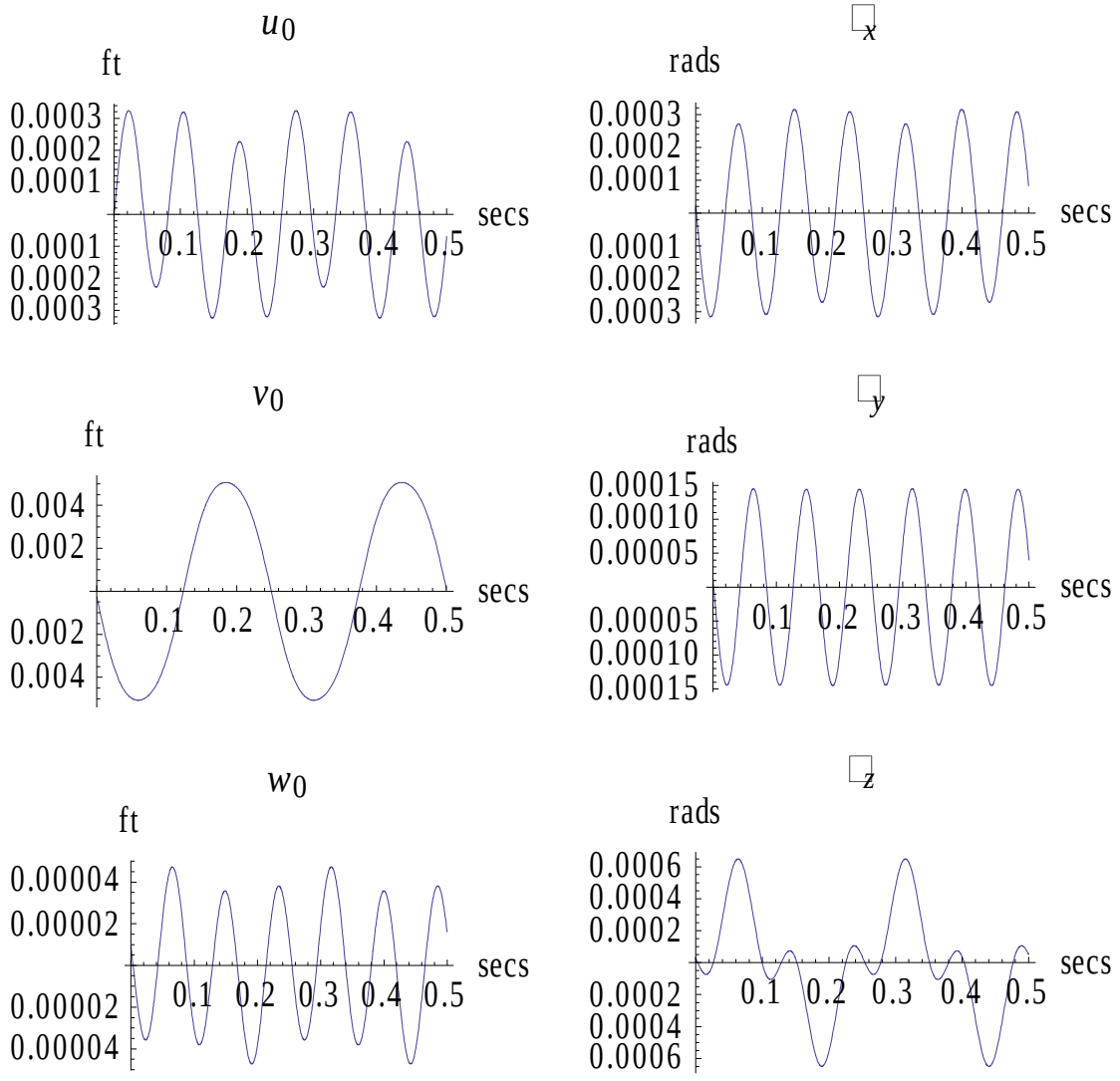

Figure 6.1 Displacement plots with $F_1(t) = 10\ \mathrm{Sin}(75t)$ at 45˚

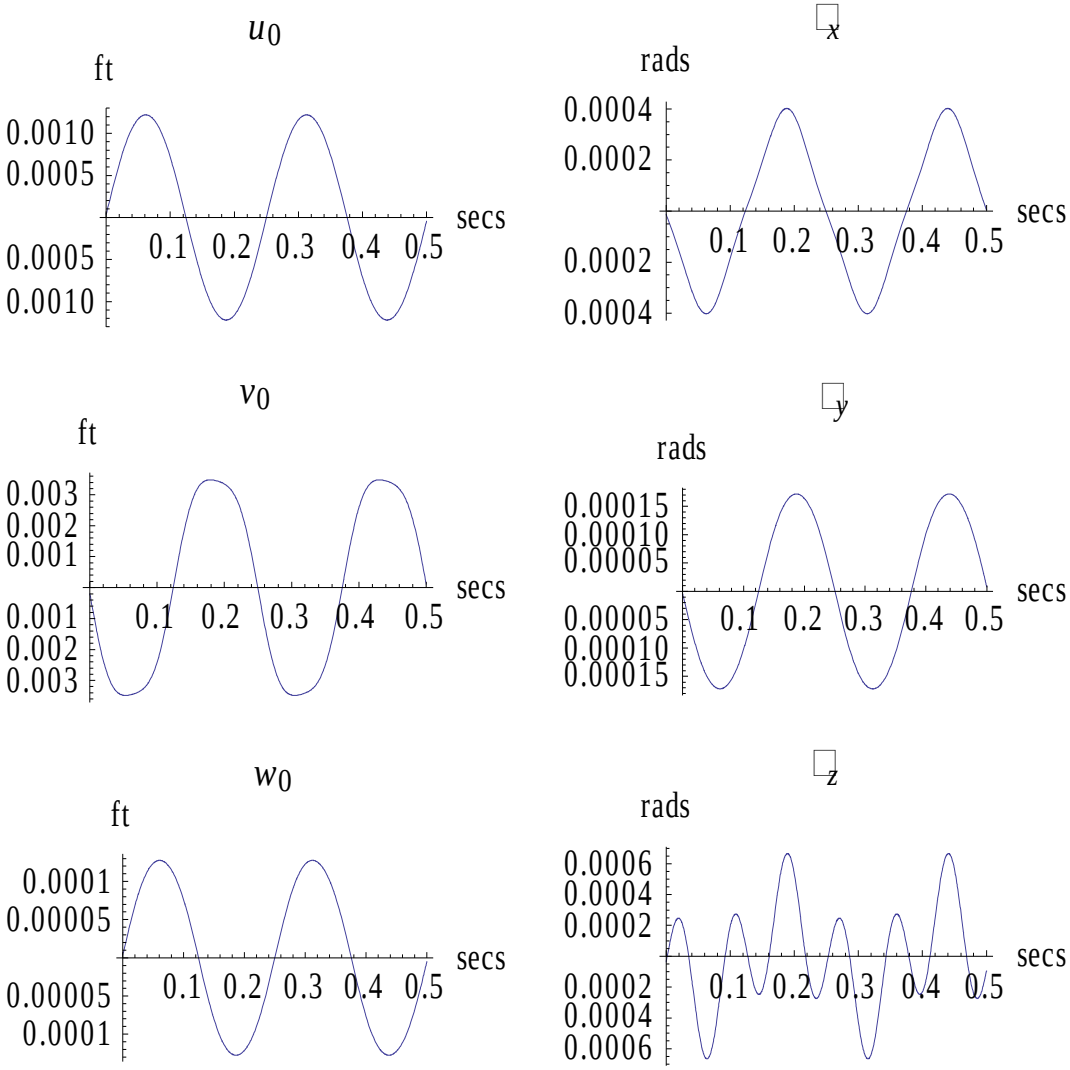

Figure 6.2 Displacement plots with $F_1(t) = 10\ \mathrm{Sin}(25t)$ at 45˚

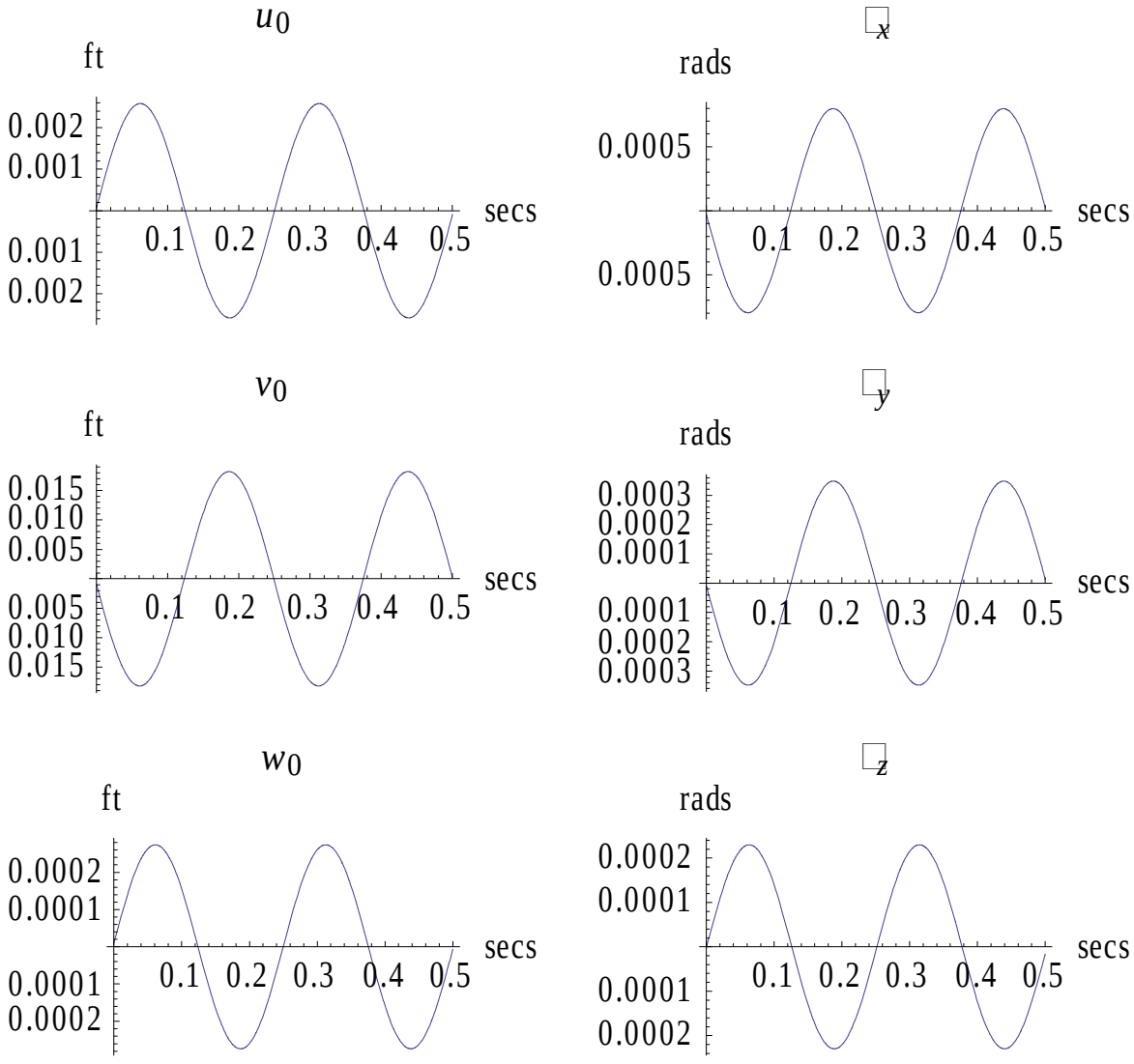

Figure 6.3 Displacement plots with $F_1(t) = F_2(t) = 10\ Sin(25t)$ at 45˚

By considering that the forcing functions were linear combinations of harmonic functions, given by

$$F_k(t) = \sum_{i=1}^{N} A_{ki} Sin[\omega_i t] \tag{6.8}$$

it was possible to define

$$F_1(t) = \sum_{i=1}^{N} A_{1i} Sin[\omega_i t]$$
$$F_2(t) = \sum_{i=1}^{N} A_{2i} Sin[\omega_i t] \qquad (6.9)$$

Here N is taken as 7, all of the magnitudes A_{ki} equal, and random choices of frequency were taken, which produced the following forcing functions

$$F_1(t) = 10[Sin(5.99t) + Sin(12.08t) + Sin(16.45t) + Sin(35.0t) + Sin(43.12t) + Sin(47.08t) + Sin(56.23t)]$$
$$F_1(t) = 10[Sin(11.09t) + Sin(21.77t) + Sin(24.88t) + Sin(32.76t) + Sin(41.99t) + Sin(47.93t) + Sin(60.22t)]$$

Figures 6.4 and 6.5 show time history plots of forcing functions F_1 and F_2.

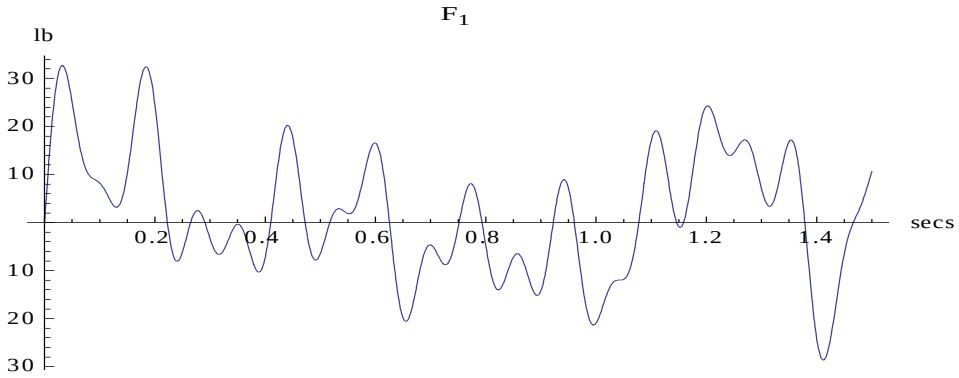

Figure 6.4 Plot of forcing function $F_1(t)$

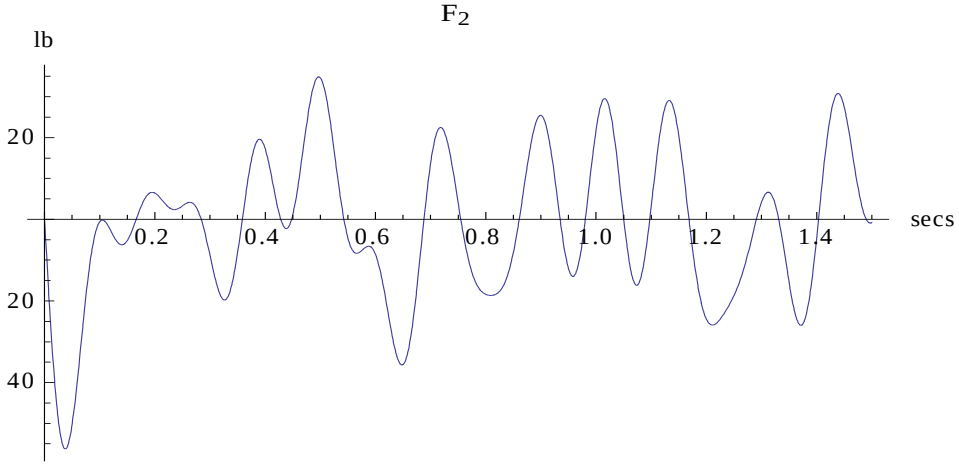

Figure 6.5 Plot of forcing function $F_2(t)$

The solution process for this case merely required a superimposed solution in modal space and a modal transformation back to the original coordinate system. The results were quite lengthy and shown only graphically below in figure 6.6

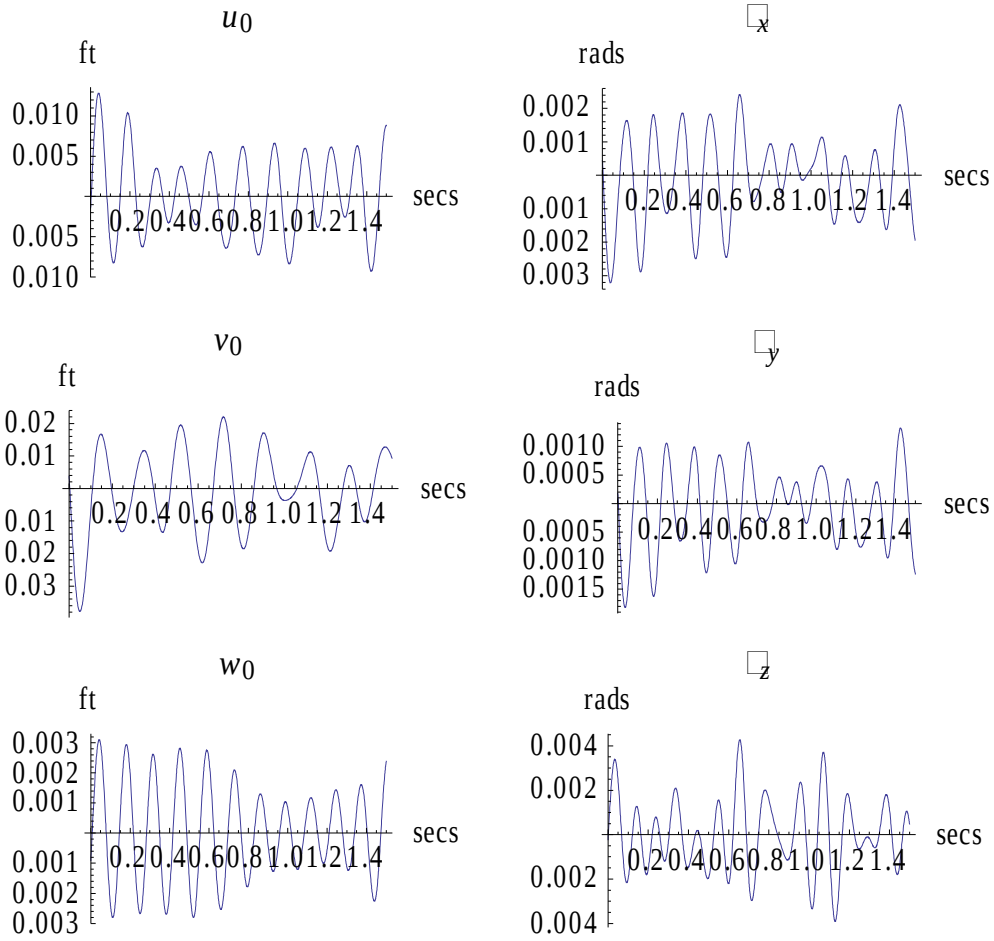

Figure 6.6 Displacement plot for multiple frequency forcing functions

CHAPTER 7

CONCLUSION AND FUTURE WORK

This project studied the analysis of an optical platform modeled as an elastically point supported plate containing discrete mass. The study consisted of free vibration, impact analysis and force vibration. Both undamped and damped cases were considered, where the damped cases were modeled using proportional damping.

1. Dynamic vibration equations of equilibrium were derived using Lagrange's Equation.
2. Undamped and damped analysis was considered
3. Two types of motion can result – Direct motion due to initial conditions and induced motion due to system characteristics. Induced motion resembles vibrational beating – slow amplitude changes with rapid oscillations.
4. Equal spring stiffness results in harmonic motion, without beating phenomena
5. Unequal spring stiffnesses induce motion in other directions
6. Unequal spring stiffnesses separate modes of vibration
7. Added masses reduce frequencies
8. Target plot density is greater with equal spring stiff nesses than when unequal.
9. Explicit expressions for all kinematic variables are known, leading to computation of velocities (linear and angular), acceleartions (linear and angular) at any point on the plate.
10. All experimental results can be compared with analytical results

There are several ideas that can be considered to extend the work of this project.

1. Compare analytical results with experimental results

2. Understand strategy to distribute force intensity for multiple frequency case
3. Develop state space representation for future control applications
4. Incorporate modeling of devices such as fast steering mirror, etc.

BIBLIOGRAPHY

1. Cox, H.L, Boxer, J., " Vibration of Rectangular Plates Point Supported at the Corners", The Aeronautical Quaterly, 1959, pp. 41 – 50.

2. Amba-Rao, C. L., "On the Vibration of a Rectangular Plate Carrying a Concentrated Mass", Transactions of the ASME, Journal of Applied Mechanics, 1964, pp. 550-551

3. Kersten, J.G.M.,"Vibration of a Rectangular Plate Supported at an Arbitrary Number of Points", J. Sound and Vibration, Vol 65, No. 4, 1979, pp. 493-504.

4. Lee, L. T., Lee., D. C.," Free Vibration of Rectangular Plates on Elastic Point Supports with the Application of a New Type of Admissible Function", Computer & Structures, No. 2, 1997, pp. 149-156.

5. Kim, C.S., Dickinson, S.M.," The Flexural Vibration of Rectangular Plates With Point Supports", J. Sound and Vibration, Vol 117, No. 2, 1987, pp. 249 – 261.

6. Kocaturk, T, Sezer, S., Demir, " Determination of the Steady State Response of Viscoelastically Point-Supported Rectangular Specially Orthotropic Plates with Added Concentrated Masses, J. Sound and Vibration, Vol 278, 2004, pp. 789 – 806.

7. Nieves, F. J., Gascon, F., Bayon, A." Natural Frequencies and Mode Shapes of Flexural Vibration of Plates: Laser Interferometry Detection and Solutions by Ritz Methods", J. Sound and Vibration, Vol 278, 2004, pp. 637 – 655..

8. Lee, C. R., Kam, T. Y., "Identification of Mechanical Properties of Elastically Restrained Laminated Composite Plates Using Vibration Data", J. Sound and Vibration, Vol 295, 2006, pp. 999 – 1061.

9. Abrate, S. (1995). Vibration of Point-Supported Rectangular Composite Plates. *Composites Science and Technology*, *53*, 325-332.

10. Adhikari, S. (2006). Damping modelling using generalized proportional damping. *Journal of Sound and Vibration, 293*, 156-170.

11. Altekin, M. (2008). Free linear vibration and buckling of super-elliptical plates resting symmetrically distributed point-supports on the diagonals. *ScienceDirect*, *46*, 1066-1086.

12. Avalos, D. R., & Larrondo, H. A. (1997). Comments on "Use of the Analytical and Numerical Combined Method in the Free Vibration Analysis of a Rectangular Plate With Any Number of Point Masses and Translational Springs". *Journal of Sound and Vibration*, *207*(4), 591-592.

13. Caughey, T. K., & O'Kelly, M. E. (1961). Effect of Damping on the Natural Frequencies

of Linear Dynamic Systems. *The Journal of the Acoustical Society of America, 33*(11), 1458-1461.

14. Cha, P. D. (1997). Free Vibration of a Rectangular Plate Carrying a Concentrated Mass. *Journal of Sound and Vibration, 207*(4), 593-596.

15. Cox, H. L., & Boxer, J. (1960). Vibration of Rectangular Plates Point-Supported at the Corners. *The Aeronautical Quarterly*, 41-50.

16. Dickinson, S. M. (1982). On the Use of Simply Supported Plate Functions in the Rayleigh-Ritz Method Applied to the Flexural Vibration of Rectangular Plates. *Journal of Sound and Vibration, 80*(2), 292-297.

17. Dickinson, S. M. (1982). On the Use of Simply Supported Plate Functions in the Rayleigh-Ritz Method Applied to the Flexural Vibration of Rectangular Plates. *Journal of Sound and Vibration, 80*(2), 292-297.

18. Fan, Z. (2001). Transient vibration and sound radiation of a rectangular plate with viscoelastic boundary supports. *International Journal for Numerical Methods in Engineering, 51*, 619-630.

19. Gorman, D. J. (1981). An Analytical Solution for the Free Vibration Analysis of Rectangular Plates Resting on Symmetrically Distributed Point Supports. *Journal of Sound and Vibration, 79*(4), 561-574.

20. Gorman, D. J. (2000). Free Vibration Analysis of Completely Free Rectangular Plates by the Superposition-Galerkin Method. *Journal of Sound and Vibration, 237*(5), 901-914.

21. Hartog, J. D. (1956). *Mechanical Vibrations, 4th Edition* (4th ed.). New York, NY: Crastre Press.

22. Hearmon, R. F. (1959). The Frequency of Flexural Vibration of Rectangular Orthotropic Plates With Clamped or Supported Edges. *Journal of Applied Mechanics*, 537-540.

23. Huang, M. H., & Thambiratnam, D. P. (2001). Free Vibration Analysis of REctangular Plates On Elastic Intermediate Supports. *Journal of Sound and Vibration, 240*(3), 567-580.

24. Inman, D. J. (2000). *Engineering Vibration, Second Edition* (2 ed.). Alexandria, VA: Prentice Hall.

25. John, J. D., Jakob, C. F., Vinay, T., & Qin, L. (2004). Phase Differential Angular Rate Sensor--Concept and Analysis. *IEEE SENSORS JOURNAL, 4*(4), 471-478.

26. Kocaturk, T., Sezer, S., & Demir, C. (2004). Determination of the steady state response of viscoelastically point-supported rectangular specially orthotropic plates with added concentrated masses. *Journal of Sound and Vibration, 278*, 789-806.

27. Lee, C. R., & Kam, T. Y. (2006). Identification of mechanical properties of elastically restrained laminated composite plates using vibration data. *Journal of Sound and Vibration*, *295*, 999-1016.

28. Lee, L. T., & Lee, D. C. (1997). Free Vibration of Rectangular Plates on Elastic Point Supports with the Application of a New Type of Admissible Function. *Computers & Structures*, *65*(2), 149-156.

29. Liew, K. M., & Lam, K. Y. (1994). Effects of Arbitrarily Distributed Elastic Point Constraints on Vibrational Behavior of Rectangular Plates. *Journal of Sound and Vibration*, *174*(1), 23-36.

30. McMillan, A. J., & Keane, A. J. (1997). Vibration Isolation in a Thin Rectangular Plate Using a Large Number of Optimally Positioned Point Masses. *Journal of Sound and Vibration*, *202*(2), 219-234.

APPENDIX A1

EXPLICIT EQUATIONS

A1.1 Coupled Dynamic Equation for Inertial Actuators

$$M_{s1t}\frac{d^2u_{s1}}{dt^2}+C_{s1}\frac{du_{s1}}{dt}+K_{s1}u_{s1}-K_{s1}(u_0(t)+z_{s1}\theta_y(t)-y_{s1}\theta_z(t)) - C_{s1}(\frac{du_0(t)}{dt}+z_{s1}\frac{d\theta_y(t)}{dt}-y_{s1}\frac{d\theta z(t)}{dt})=F_{slx} \tag{A1.1}$$

$$M_{s1t}\frac{d^2v_{s1}}{dt^2}+C_{s1}\frac{dv_{s1}}{dt}+K_{s1}v_{s1}-K_{s1}(v_0(t)-z_{s1}\theta_x(t)+x_{s1}\theta_z(t)) - C_{s1}(\frac{dv_0(t)}{dt}-z_{s1}\frac{d\theta_x(t)}{dt}+x_{s1}\frac{d\theta z(t)}{dt})=F_{s1y} \tag{A1.2}$$

$$M_{s2t}\frac{d^2v_{s2}}{dt^2}+C_{s2}\frac{dv_{s2}}{dt}+K_{s2}v_{s2}-K_{s2}(v_0(t)-z_{s2}\theta_x(t)+x_{s2}\theta_z(t)) - C_{s2}(\frac{dv_0(t)}{dt}-z_{s2}\frac{d\theta_x(t)}{dt}+x_{s2}\frac{d\theta_z(t)}{dt})=F_{s2y} \tag{A1.3}$$

$$M_{s2t}\frac{d^2w_{s2}}{dt^2}+C_{s2}\frac{dw_{s2}}{dt}+K_{s1}w_{s1}-K_{s2}(w_0(t)+y_{s2}\theta_x(t)-x_{s2}\theta_y(t)) - C_{s2}(\frac{dw_0(t)}{dt}+y_{s2}\frac{d\theta_x(t)}{dt}-x_{s2}\frac{d\theta_y(t)}{dt})=F_{s2z} \tag{A1.4}$$

A1.2 Coupled Dynamic Equations for Optical Platform

$$\begin{aligned}&(M_p+\sum_{i=1}^{N}M_i+\sum_{i=1}^{2}M_{sib})\frac{d^2u_0(t)}{dt^2}+(\sum_{1=i}^{4}C_i+\sum_{i=1}^{2}C_{si})\frac{du_0(t)}{dt}+(\sum_{i=1}^{4}k_i+\sum_{i=1}^{2}k_{si})u_0(t)+\\&(M_p\bar{z}+\sum_{i=1}^{N}M_iz_i+\sum_{i=1}^{2}M_{sib}z_{si})\frac{d^2\theta_y(t)}{d^2t}+(\sum_{i=1}^{4}C_iz_i+\sum_{i=1}^{2}C_{si}z_{si})\frac{d\theta_y(t)}{dt}+(\sum_{i=1}^{4}K_iz_i+\sum_{i=1}^{2}K_{si}z_{si})\theta_y(t)-\\&(\sum_{i=1}^{N}M_iy_i+\sum_{i=1}^{2}M_{sib}y_{si})\frac{d^2\theta_z(t)}{d^2t}-(\sum_{i=1}^{4}C_iy_i+\sum_{i=1}^{2}C_{si}y_{si})\frac{d\theta_z(t)}{dt}-(\sum_{i=1}^{4}K_iy_i+\sum_{i=1}^{2}K_{si}y_{si})\theta_z(t)\\&-K_{s1}u_{s1}(t)+C_{s1}\frac{du_{s1}(t)}{dt}=0\end{aligned} \tag{A1.5}$$

$$
\begin{aligned}
&(M_p+\sum_{i=1}^{N}M_i+\sum_{i=1}^{2}M_{si})\frac{d^2v_0(t)}{dt^2}+(\sum_{1=i}^{4}C_i+\sum_{i=1}^{2}C_{si})\frac{dv_0(t)}{dt}+(\sum_{i=1}^{4}k_i+\sum_{i=1}^{2}k_{si})v_0(t)-\\
&(M_p\bar{z}+\sum_{i=1}^{N}M_iz_i+\sum_{i=1}^{2}M_{si}z_{si})\frac{d^2\theta_x(t)}{dt^2}-(\sum_{i=1}^{4}C_iz_i+\sum_{i=1}^{2}C_{si}z_{si})\frac{d\theta_x(t)}{dt}-(\sum_{i=1}^{4}K_iz_i+\sum_{i=1}^{2}K_{si}z_{si})\theta_x(t)+\\
&(M_p\bar{x}+\sum_{i=1}^{N}M_ix_i+\sum_{i=1}^{2}M_{si}x_{si})\frac{d^2\theta_z(t)}{dt^2}+(\sum_{i=1}^{4}C_ix_i+\sum_{i=1}^{2}C_{si}x_{si})\frac{d\theta_z(t)}{dt}+(\sum_{i=1}^{4}K_ix_i+\sum_{i=1}^{2}K_{si}x_{si})\theta_z(t)\\
&-K_{s1}v_{s1}(t)-C_{s1}\frac{dv_{s1}(t)}{dt}-K_{s2}v_{s2}(t)-C_{s2}\frac{dv_{s2}(t)}{dt}=0
\end{aligned}
\tag{A1.6}
$$

$$
\begin{aligned}
&(M_p+\sum_{i=1}^{N}M_i+\sum_{i=1}^{2}M_{si})\frac{d^2w_0(t)}{dt^2}+(\sum_{1=i}^{4}C_i+\sum_{i=1}^{2}C_{si})\frac{dw_0(t)}{dt}+(\sum_{i=1}^{4}k_i+\sum_{i=1}^{2}k_{si})w_0(t)+\\
&(\sum_{i=1}^{N}M_iy_i+\sum_{i=1}^{2}M_{si}y_{si})\frac{d^2\theta_x(t)}{d^2t}+(\sum_{i=1}^{4}C_iy_i+\sum_{i=1}^{2}C_{si}y_{si})\frac{d\theta_x(t)}{dt}+(\sum_{i=1}^{4}K_iy_i+\sum_{i=1}^{2}K_{si}y_{si})\theta_x(t)-\\
&(M_p\bar{x}+\sum_{i=1}^{N}M_ix_i+\sum_{i=1}^{2}M_{si}x_{si})\frac{d^2\theta_y(t)}{d^2t}-(\sum_{i=1}^{4}C_ix_i+\sum_{i=1}^{2}C_{si}x_{si})\frac{d\theta_y(t)}{dt}-(\sum_{i=1}^{4}K_ix_i+\sum_{i=1}^{2}K_{si}x_{si})\theta_y(t)\\
&-K_{s2}w_{s2}(t)-C_{s2}\frac{dw_{s2}(t)}{dt}=0
\end{aligned}
\tag{A1.7}
$$

$$
\begin{aligned}
&(I_{xx}+\sum_{i=1}^{N}M_i(y_i^2+z_i^2)+\sum_{i=1}^{2}M_{si}(y_{zsi}^2+z_{zsi}^2))\frac{d^2\theta_x(t)}{dt^2}+(\sum_{i=1}^{4}C_i(y_i^2+z_i^2)+\sum_{i=1}^{2}C_{si}(y_{zsi}^2+z_{zsi}^2))\frac{d\theta_x(t)}{dt}+\\
&(\sum_{i=1}^{4}K_i(y_i^2+z_i^2)+\sum_{i=1}^{2}K_{si}(y_{zsi}^2+z_{zsi}^2))\theta_x(t)-\\
&(\sum_{i=1}^{N}M_ix_iy_i+\sum_{i=1}^{2}M_{si}x_{si}y_{si})\frac{d^2\theta_y(t)}{dt^2}-(\sum_{i=1}^{4}C_ix_iy_i+\sum_{i=1}^{2}C_{si}x_{si}y_{si})\frac{d\theta_y(t)}{dt}-(\sum_{i=1}^{4}K_ix_iy_i+\sum_{i=1}^{2}K_{si}x_{si}y_{si})\theta_y(t)-\\
&(M_p\bar{z}+\sum_{i=1}^{N}M_iz_i+\sum_{i=1}^{2}M_{si}z_{si})\frac{d^2v_0(t)}{dt^2}-(\sum_{i=1}^{4}C_iz_i+\sum_{i=1}^{2}C_{si}z_{si})\frac{dv_0(t)}{dt}-(\sum_{i=1}^{4}K_iz_i+\sum_{i=1}^{2}K_{si}z_{si})v_0(t)+\\
&(\sum_{i=1}^{N}M_iy_i+\sum_{i=1}^{2}M_{si}y_{si})\frac{d^2w_0(t)}{dt^2}+(\sum_{i=1}^{4}C_iy_i+\sum_{i=1}^{2}C_{si}y_{si})\frac{dw_0(t)}{dt}+(\sum_{i=1}^{4}K_iz_i+\sum_{i=1}^{2}K_{si}z_{si})w_0(t)-\\
&(I_{xz}+\sum_{i=1}^{N}M_ix_iz_i+\sum_{i=1}^{2}M_{si}x_{si}z_{si})\frac{d^2\theta_z(t)}{dt^2}-(\sum_{i=1}^{4}C_ix_iz_i+\sum_{i=1}^{2}C_{si}x_{si}z_{si})\frac{d\theta_z(t)}{dt}-(\sum_{i=1}^{4}K_ix_iz_i+\sum_{i=1}^{2}K_{si}x_{si}z_{si})\theta_z(t)+\\
&K_{s1}z_{s1}v_{s1}(t)+C_{s1}z_{s1}\frac{dv_{s1}(t)}{dt}+K_{s2}z_{s2}v_{s2}(t)+C_{s2}z_{s2}\frac{dv_{s2}(t)}{dt}=0
\end{aligned}
\tag{A1.8}
$$

$$
\begin{aligned}
&(I_{yy}+\sum_{i=1}^{N}M_i(x_i^2+z_i^2)+\sum_{i=1}^{2}M_{si}(x_{zsi}^2+z_{zsi}^2))\frac{d^2\theta_y(t)}{dt^2}+(\sum_{i=1}^{4}C_i(x_i^2+z_i^2)+\sum_{i=1}^{2}C_{si}(x_{si}^2+z_{si}^2))\frac{d\theta_y(t)}{dt}+\\
&(\sum_{i=1}^{4}K_i(x_i^2+z_i^2)+\sum_{i=1}^{2}K_{si}(x_{si}^2+z_{si}^2))\theta_y(t)-\\
&(\sum_{i=1}^{N}M_ix_iy_i+\sum_{i=1}^{2}M_{si}x_{si}y_{si})\frac{d^2\theta_x(t)}{dt^2}-(\sum_{i=1}^{4}C_ix_iy_i+\sum_{i=1}^{2}C_{si}x_{si}y_{si})\frac{d\theta_x(t)}{dt}-\\
&(\sum_{i=1}^{4}K_ix_iy_i+\sum_{i=1}^{2}K_{si}x_{si}y_{si})\theta_x(t)-\\
&(\sum_{i=1}^{N}M_iy_iz_i+\sum_{i=1}^{2}M_{si}y_{si}z_{si})\frac{d^2\theta_z(t)}{dt^2}-(\sum_{i=1}^{4}C_iy_iz_i+\sum_{i=1}^{2}C_{si}y_{si}z_{si})\frac{d\theta_z(t)}{dt}-\\
&(\sum_{i=1}^{4}K_iy_iz_i+\sum_{i=1}^{2}K_{si}y_{si}z_{si})\theta_z(t)+\\
&(M_p\bar{z}+\sum_{i=1}^{N}M_iz_i+\sum_{i=1}^{2}M_{si}z_{si})\frac{d^2u_0(t)}{dt^2}+(\sum_{i=1}^{4}C_iz_i+\sum_{i=1}^{2}C_{si}z_{si})\frac{du_0(t)}{dt}+(\sum_{i=1}^{4}K_iz_i+\sum_{i=1}^{2}K_{si}z_{si})u_0(t)-\\
&(M_p\bar{x}+\sum_{i=1}^{N}M_ix_i+\sum_{i=1}^{2}M_{si}x_{si})\frac{d^2w_0(t)}{dt^2}-(\sum_{i=1}^{4}C_ix_i+\sum_{i=1}^{2}C_{si}x_{si})\frac{dw_0(t)}{dt}-(\sum_{i=1}^{4}K_ix_i+\sum_{i=1}^{2}K_{si}x_{si})w_0(t)-\\
&K_{s1}z_{s1}u_{s1}(t)+K_{s2}x_{s2}w_{s2}(t)-C_{s1}z_{s1}\frac{du_{s1}(t)}{dt}+C_{s2}x_{s2}\frac{dw_{s2}(t)}{dt}=0
\end{aligned}
\tag{A1.9}
$$

$$
\begin{aligned}
&(I_{zz}+\sum_{i=1}^{N}M_i(x_i^2+y_i^2)+\sum_{i=1}^{2}M_{si}(x_{zsi}^2+y_{zsi}^2))\frac{d^2\theta_z(t)}{dt^2}+(\sum_{i=1}^{4}C_i(x_i^2+y_i^2)+\sum_{i=1}^{2}C_{si}(x_{zsi}^2+y_{zsi}^2)\frac{d\theta_z(t)}{dt}+\\
&(\sum_{i=1}^{4}K_i(x_i^2+y_i^2)+\sum_{i=1}^{2}K_{si}(x_{zsi}^2+y_{zsi}^2))\theta_z(t)+\\
&(M_p\bar{x}+\sum_{i=1}^{N}M_ix_i+\sum_{i=1}^{2}M_{si}x_{si})\frac{d^2v_0(t)}{dt^2}+(\sum_{i=1}^{4}C_ix_i+\sum_{i=1}^{2}C_{si}x_{si})\frac{dv_0(t)}{dt}+(\sum_{i=1}^{4}K_ix_i+\sum_{i=1}^{2}K_{si}x_{si})v_0(t)-\\
&(\sum_{i=1}^{N}M_iy_i+\sum_{i=1}^{2}M_{si}y_{si})\frac{d^2u_0(t)}{dt^2}-(\sum_{i=1}^{4}C_iy_i+\sum_{i=1}^{2}C_{si}y_{si})\frac{du_0(t)}{dt}-(\sum_{i=1}^{4}K_iy_i+\sum_{i=1}^{2}K_{si}y_{si})u_0(t)-\\
&(I_{xz}+\sum_{i=1}^{N}M_ix_iz_i+\sum_{i=1}^{2}M_{si}x_{si}z_{si})\frac{d^2\theta_x(t)}{dt^2}-(\sum_{i=1}^{4}C_ix_iz_i\sum_{i=1}^{2}C_{si}x_{si}z_{si})\frac{d\theta_x(t)}{dt}-(\sum_{i=1}^{4}K_ix_iz_i+\sum_{i=1}^{2}K_{si}x_{si}z_{si})\theta_x(t)-\\
&(\sum_{i=1}^{N}M_iy_iz_i+\sum_{i=1}^{2}M_{si}y_{si}z_{si})\frac{d^2\theta_y(t)}{dt^2}-(\sum_{i=1}^{4}C_iy_iz_i\sum_{i=1}^{2}C_{si}y_{si}z_{si})\frac{d\theta_y(t)}{dt}-(\sum_{i=1}^{4}K_iy_iz_i+\sum_{i=1}^{2}K_{si}y_{si}z_{si})\theta_y(t)+\\
&K_{s1}y_{s1}u_{s1}(t)-K_{s1}x_{s1}v_{s1}(t)-K_{s2}x_{s2}v_{s2}(t)+C_{s1}y_{s1}\frac{du_{s1}(t)}{dt}-C_{s1}x_{s1}\frac{dv_{s1}(t)}{dt}-C_{s2}x_{s2}\frac{dv_{s2}(t)}{dt}=0
\end{aligned}
\tag{A1.10}
$$

APPENDIX A2

SUB MATRICIES

A2.1 Introduction

This appendix presents explicit forms of the matrices used. Recall that Lagrange's Equation provides a means of obtaining a system's governing equations of motion, which in matrix form become

$$[m]\{\ddot{x}\}+[c]\{\dot{x}\}+[k]\{x\}=\{F\} \tag{A2.1}$$

Each matrix in eqn. A2.1 is subdivided into four matrices,

$$\begin{bmatrix}[m_s]_{(4x4)} & [0]_{(4x6)}\\ [0]_{(6x4)} & [m_p]_{(6x6)}\end{bmatrix}\begin{Bmatrix}\{\ddot{q}_s\}_{(4x1)}\\ \{\ddot{q}_p\}_{(6x1)}\end{Bmatrix}+\begin{bmatrix}[c_s]_{(4x4)} & [c_{ps}]_{(4x6)}\\ [c_{sp}]_{(6x4)} & [c_p]_{(6x6)}\end{bmatrix}\begin{Bmatrix}\{\dot{q}_s\}_{(4x1)}\\ \{\dot{q}_p\}_{(6x1)}\end{Bmatrix}$$
$$+\begin{bmatrix}[k_s]_{(4x4)} & [k_{ps}]_{(4x6)}\\ [k_{sp}]_{(6x4)} & [k_p]_{(6x6)}\end{bmatrix}\begin{Bmatrix}\{q_s\}_{(4x1)}\\ \{q_p\}_{(6x1)}\end{Bmatrix}=\begin{Bmatrix}\{Q_s\}_{(4x1)}\\ \{0\}_{(6x1)}\end{Bmatrix} \tag{2.16}$$

where $[m_s]_{(4x4)}$ is the mass matrix of the shakers, $[m_p]_{(6x6)}$ is the mass matrix for the plate, and its discrete masses, $[c_s]_{(4x4)}$ is the damping matrix of the shakers, $[c_{ps}]_{(4x6)}$ is the damping matrix that couples the motion of the plate and the shakers, $[k_s]_{(4x4)}$ is the stiffness matrix of the shakers, $[k_{ps}]_{(4x6)}$ is the stiffness matrix which couples the motion of the plate and the shakers, $[k_p]_{(6x6)}$ is the stiffness matrix of the plate, $\begin{Bmatrix}\{\ddot{q}_s\}_{(4x1)}\\ \{\ddot{q}_p\}_{(6x1)}\end{Bmatrix}$ is a vector of the shaker and plate accelerations, $\begin{Bmatrix}\{\dot{q}_s\}_{(4x1)}\\ \{\dot{q}_p\}_{(6x1)}\end{Bmatrix}$ is a vector of the shaker and plate velocities, $\begin{Bmatrix}\{q_s\}_{(4x1)}\\ \{q_p\}_{(6x1)}\end{Bmatrix}$ is a vector of the shaker and plate displacements, and $\begin{Bmatrix}\{Q_s\}_{(4x1)}\\ \{0\}_{(6x1)}\end{Bmatrix}$ is a vector comprised of the forces imparted by the shakers onto the system.

The above defined matrices for the shaker are

$$[m_s] = \begin{bmatrix} m_{s1t} & 0 & 0 & 0 \\ 0 & m_{s1t} & 0 & 0 \\ 0 & 0 & m_{s2t} & 0 \\ 0 & 0 & 0 & m_{s2t} \end{bmatrix}$$

$$[c_s] = \begin{bmatrix} c_{s1} & 0 & 0 & 0 \\ 0 & c_{s1} & 0 & 0 \\ 0 & 0 & c_{s2} & 0 \\ 0 & 0 & 0 & c_{s2} \end{bmatrix}$$

$$[k_s] = \begin{bmatrix} k_{s1} & 0 & 0 & 0 \\ 0 & k_{s1} & 0 & 0 \\ 0 & 0 & k_{s2} & 0 \\ 0 & 0 & 0 & k_{s2} \end{bmatrix}$$

Here s1 and s2 stand for shaker 1 and 2 and t represents the portion of the mass of the shaker in motion. The matrices that couple the motion of the shaker and the plate are

$$[c_{ps}] = [c_{sp}]^T = \begin{bmatrix} -c_{s1} & 0 & 0 & \\ 0 & -c_{s1} & -c_{s2} & 0 \\ 0 & 0 & 0 & -c_{s2} \\ 0 & c_{s1}z_{s1} & c_{s2}z_{s2} & -c_{s2}y_{s2} \\ -c_{s1}z_{s1} & 0 & 0 & 0 \\ c_{s1}y_{s1} & -c_{s1}x_{s1} & -c_{s2}x_{s2} & 0 \end{bmatrix}$$

$$[k_{ps}] = [k_{sp}]^T = \begin{bmatrix} -k_{s1} & 0 & 0 & \\ 0 & -k_{s1} & -k_{s2} & 0 \\ 0 & 0 & 0 & -k_{s2} \\ 0 & k_{s1}z_{s1} & k_{s2}z_{s2} & -k_{s2}y_{s2} \\ -k_{s1}z_{s1} & 0 & 0 & 0 \\ k_{s1}y_{s1} & -k_{s1}x_{s1} & -k_{s2}x_{s2} & 0 \end{bmatrix}$$

The matrices that govern the motion of the plate are

$$[k_p]=\begin{bmatrix} \sum_{i=1}^{N} k_i & 0 & 0 & 0 & \sum_{i=1}^{N} k_i z_i & \sum_{i=1}^{N} k_i y_i \\ 0 & \sum_{i=1}^{N} k_i & 0 & \sum_{i=1}^{N} k_i z_i & 0 & \sum_{i=1}^{N} k_i x_i \\ 0 & 0 & \sum_{i=1}^{N} k_i & \sum_{i=1}^{N} k_i y_i & \sum_{i=1}^{N} k_i x_i & 0 \\ 0 & \sum_{i=1}^{N} k_i z_i & \sum_{i=1}^{N} k_i y_i & \sum_{i=1}^{N} k_i y_i^2 & -\sum_{i=1}^{N} k_i x_i y_i & \sum_{i=1}^{N} k_i x_i z_i \\ \sum_{i=1}^{N} k_i z_i & 0 & \sum_{i=1}^{N} k_i x_i & -\sum_{i=1}^{N} k_i x_i z_i & \sum_{i=1}^{N} k_i x_i^2 & \sum_{i=1}^{N} k_i y_i z_i \\ \sum_{i=1}^{N} k_i y_i & \sum_{i=1}^{N} k_i x_i & 0 & \sum_{i=1}^{N} k_i x_i z_i & \sum_{i=1}^{N} k_i y_i z_i & \sum_{i=1}^{N} k_i y_i^2 \end{bmatrix}$$

$$[c_p]=\begin{bmatrix} \sum_{i=1}^{N} c_i & 0 & 0 & 0 & \sum_{i=1}^{N} c_i z_i & \sum_{i=1}^{N} c_i y_i \\ 0 & \sum_{i=1}^{N} c_i & 0 & \sum_{i=1}^{N} c_i z_i & 0 & \sum_{i=1}^{N} c_i x_i \\ 0 & 0 & \sum_{i=1}^{N} c_i & \sum_{i=1}^{N} c_i y_i & \sum_{i=1}^{N} c_i x_i & 0 \\ 0 & \sum_{i=1}^{N} c_i z_i & \sum_{i=1}^{N} c_i y_i & \sum_{i=1}^{N} c_i y_i^2 & -\sum_{i=1}^{N} c_i x_i y_i & \sum_{i=1}^{N} c_i x_i z_i \\ \sum_{i=1}^{N} c_i z_i & 0 & \sum_{i=1}^{N} c_i x_i & -\sum_{i=1}^{N} c_i x_i z_i & \sum_{i=1}^{N} c_i x_i^2 & \sum_{i=1}^{N} c_i y_i z_i \\ \sum_{i=1}^{N} c_i y_i & \sum_{i=1}^{N} c_i x_i & 0 & \sum_{i=1}^{N} c_i x_i z_i & \sum_{i=1}^{N} c_i y_i z_i & \sum_{i=1}^{N} c_i y_i^2 \end{bmatrix}$$

$$[m_p]=\begin{bmatrix} m_p+\sum_{i=1}^{N} m_i & 0 & 0 & 0 & m_p\bar{z}+\sum_{i=1}^{N} m_i z_i & -m_p\bar{y}-\sum_{i=1}^{N} m_i y_i \\ 0 & m_p+\sum_{i=1}^{N} m_i & 0 & -m_p\bar{z}-\sum_{i=1}^{N} m_i z_i & 0 & m_p\bar{x}+\sum_{i=1}^{N} m_i x_i \\ 0 & 0 & m_p+\sum_{i=1}^{N} m_i & m_p\bar{y}+\sum_{i=1}^{N} m_i y_i & -m_p\bar{x}-\sum_{i=1}^{N} m_i x_i & 0 \\ 0 & -m_p\bar{z}-\sum_{i=1}^{N} m_i z_i & m_p\bar{y}+\sum_{i=1}^{N} m_i y_i & I_{xx}+\sum_{i=1}^{N} m_i y_i^2 & -\sum_{i=1}^{N} m_i x_i y_i & -I_{xy}-I_{xz}-\sum_{i=1}^{N} m_i x_i z_i \\ m_p\bar{z}+\sum_{i=1}^{N} m_i z_i & 0 & -m_p\bar{x}-\sum_{i=1}^{N} m_i x_i & -\sum_{i=1}^{N} m_i x_i z_i & I_{yy}+\sum_{i=1}^{N} m_i x_i^2 & -I_{yz}-\sum_{i=1}^{N} m_i y_i z_i \\ -m_p\bar{y}-\sum_{i=1}^{N} m_i y_i & m_p\bar{x}+\sum_{i=1}^{N} m_i x_i & 0 & -I_{xy}-I_{xz}-\sum_{i=1}^{N} m_i x_i z_i & -I_{yz}-\sum_{i=1}^{N} m_i y_i z_i & I_{zz}+\sum_{i=1}^{N} m_i y_i^2 \end{bmatrix}$$

APPENDIX B1

MATHEMATICA CODE FOR FORCED VIBRATION ANALYSIS

```
ClearAll;
(*input*)
fs1x = 7.071;
fs1y=-7.071;
fs2y=-10;
tf=1.5;
ω11 = 5.99;
ω12 = 12.08;
ω13 = 16.45;
ω14 = 35.00;
ω15 = 43.12;
ω16 = 47.08;
ω17 = 75.0;
ω21= 11.09;
ω22 = 21.77;
ω23 = 24.88;
ω24 = 32.76;
ω25 = 41.99;
ω26 = 47.93;
ω27 = 60.22;
(*Stiffness Terms*)
α=0.0007812;
β=0.0007812;
k1=115*12;
(*k1=1612.5
k2=1612.5
k3=1612.5
k4=1612.5*)
k3=120*12;
k2=110*12;
k4=105*12;
(*k1=105*12;
k2=125*12;
k3=110*12;
k4=115*12;*)
ks1 = 3689.27;
ks2=3689.27;
mp=4.658;
ma=0.155;(*m1*)
mj=0.078;(*m2*)
ml= 0.100;(*m3*)
ml2=0.233;(*m4*)
mts1= 0.086335;
mts2= 0.086335;
```

```
mbs1= 0.098447;
mbs2= 0.098447;
(*mp=1.310488015;*)
mtotal=ma+mj+ml+ml2+mts1+mts2+mbs1+mbs2+mp;
(*xl = 0.0 ;
zl = 0.0;
yl= 0.0;
xl2 = 0.0;
zl2 = 0.0;
yl2 = 0.0;
xa =0.0;
za = 0.0;
ya = 0.0;
xj =0.0;
zj = 0.0;
yj = 0.0;*)

xl = -15/12; (*(6/7)*(1/2)*lplate;*)
zl = -15/12; (*(6/7)*(1/2)*wplate;*)
yl= (1/2)*hplate+0.333;
xl2 = 6/12; (*(6/7)*(1/2)*lplate;*)
zl2 = -6/12; (*(6/7)*(1/2)*wplate;*)
yl2 = (1/2)*hplate+0.333;
xa =9/12;
za = 9/12;
ya = (1/2)*hplate+0.333;
xj =-12/12;
zj = 12/12;
yj = (1/2)*hplate+0.333;

xs1 =0; (*(6/7)*(1/2)*lplate;*)
zs1 =-(2/7)*(1/2)*wplate;
ys1 =(1/2)*hplate+0.333;

xs2 = -(2/7)*(1/2)*lplate;
zs2 =0
ys2 =(1/2)*hplate+0.333;

xbs1 =0; (*(6/7)*(1/2)*lplate;*)
zbs1 =-(2/7)*(1/2)*wplate;
ybs1 =(1/2)*hplate;

xbs2 =-(2/7)*(1/2)*lplate;
zbs2 =0
ybs2 =(1/2)*hplate;

lplate=36/12;
wplate=36/12;
hplate = 2/12;
Ixx =(mp/12)*(lplate^2+hplate^2);
Izz = (mp/12)*(wplate^2+hplate^2);
Iyy = (mp/12)*(lplate^2+wplate^2);
Ixz = 0;
Ixy = 0;
```

```
Iyz = 0;
zbar = 0;
xbar = 0;
ybar = 0;
lspring=17.25/12;
wspring = 17.25/12;
hspring = (1/2)*hplate;
z1 = lspring;
y1  = -hspring;
x1 = wspring;
z2 = lspring;
y2 = -hspring;
x2 = -wspring;
z3 = -lspring;
y3 = -hspring;
x3 = -wspring;
z4 = -lspring;
y4 = -hspring;
x4 = wspring;
position={us1[t],vs1[t],vs2[t],u0[t],v0[t],w0[t],θx[t],θy[t],θz[t
]};
velocity={us1'[t],vs1'[t],vs2'[t],u0'[t],v0'[t],w0'[t],θx'[t],θy'
[t],θz'[t]};
acceleration={us1''[t],vs1''[t],vs2''[t],u0''[t],v0''[t],w0''[t],
θx''[t],θy''[t],θz''[t]};
(*force={fs1x*Sin[ω1*t],fs1y*Sin[ω1*t],fs2y*Sin[ω2*t],fs2z*Sin[ω
2*t],0,0,0,0,0,0};*)
F={fs1x*(Sin[ω11*t]+Sin[ω12*t]+Sin[ω13*t]+Sin[ω14*t]+Sin[ω15*t]+
Sin[ω16*t]+Sin[ω17*t]),fs1y*(Sin[ω11*t]+Sin[ω12*t]+Sin[ω13*t]+Si
n[ω14*t]+Sin[ω15*t]+Sin[ω16*t]+Sin[ω17*t]),fs2y*(Sin[ω21*t]+Sin[
ω22*t]+Sin[ω23*t]+Sin[ω24*t]+Sin[ω25*t]+Sin[ω26*t]+Sin[ω27*t]),0
,0,0,0,0,0}
B={{1,0,0,0,0,0,0,0,0,0},{0,1,0,0,0,0,0,0,0,0},{0,0,1,0,0,0,0,0,
0,0},{0,0,0,0,0,0,0,0,0,0},{0,0,0,0,0,0,0,0,0,0},{0,0,0,0,0,0,0,
0,0,0},{0,0,0,0,0,0,0,0,0,0},{0,0,0,0,0,0,0,0,0,0},{0,0,0,0,0,0
,0,0,0,0}};
KE1=(1/2)*mts1*((us1'[t])^2+(vs1'[t])^2);
KE2=(1/2)*mts2*((vs2'[t])^2);
(* Kinetic Energy of the Moving Masses of Actuators*)
(* Potential Energy of the Springs Attached to Actuators*)
PE1=(ks1/2)*((us1[t]-(u0[t]+zs1*θy[t]-ys1*θz[t]))^2+(vs1[t]-
(v0[t]-zs1*θx[t]+xs1*θz[t]))^2+(w0[t]-xs1*θy[t]+ys1*θx[t])^2);
PE2=(ks2/2)*((u0[t]+zs2*θy[t]-ys2*θz[t])^2+(vs2[t]-(v0[t]-
zs2*θx[t]+xs2*θz[t]))^2+((w0[t]-xs2*θy[t]+ys2*θx[t]))^2);
(* Potential Energy of the Springs Attached to Actuators*)
(* Potential Energy of the Springs Attached to Actuators*)
RD1=(cs1/2)*((us1'[t]-(u0'[t]+zs1*θy'[t]-y1*θz'[t]))^2+(vs1'[t]-
(v0'[t]-zs1*θx'[t]+xs1*θz'[t]))^2+(w0'[t]-
xs1*θy'[t]+ys1*θx'[t])^2);
```

```
RD2=(cs2/2)*((u0'[t]+zs2*θy'[t]-ys2*θz'[t])^2+(vs2'[t]-(v0'[t]-
zs2*θx'[t]+xs2*θz'[t]))^2+((w0'[t]-xs2*θy'[t]+ys2*θx'[t]))^2);
(* Potential Energy of the Springs Attached to Actuators*)
KE=(ml/2)*((u0'[t]+zl*θy'[t]-yl*θz'[t])^2+(v0'[t]-
zl*θx'[t]+xl*θz'[t])^2+(w0'[t]-xl*θy'[t]+yl*θx'[t])^2)+
   (ml2/2)*((u0'[t]+zl2*θy'[t]-yl2*θz'[t])^2+(v0'[t]-
zl2*θx'[t]+xl2*θz'[t])^2+(w0'[t]-xl2*θy'[t]+yl2*θx'[t])^2)+
   (mj/2)*((u0'[t]+zj*θy'[t]-yj*θz'[t])^2+(v0'[t]-
zj*θx'[t]+xj*θz'[t])^2+(w0'[t]-xj*θy'[t]+yj*θx'[t])^2)+
   (ma/2)*((u0'[t]+za*θy'[t]-ya*θz'[t])^2+(v0'[t]-
za*θx'[t]+xa*θz'[t])^2+(w0'[t]-xa*θy'[t]+ya*θx'[t])^2)+
   (mbs1/2)*((u0'[t]+zbs1*θy'[t]-ybs1*θz'[t])^2+(v0'[t]-
zbs1*θx'[t]+xbs1*θz'[t])^2+(w0'[t]-xbs1*θy'[t]+ybs1*θx'[t])^2)+
   (mbs2/2)*((u0'[t]+zbs2*θy'[t]-ybs2*θz'[t])^2+(v0'[t]-
zbs2*θx'[t]+xbs2*θz'[t])^2+(w0'[t]-xbs2*θy'[t]+ybs1*θx'[t])^2)+

(mp/2)*((u0'[t])^2+(v0'[t])^2+(w0'[t])^2)+mp*xbar*(v0'[t]*θz'[t]-
w0'[t]*θy'[t])+mp*zbar*(u0'[t]*θy'[t]-
v0'[t]*θx'[t])+(1/2)*(Iyy*(θy'[t])^2+Ixx*(θx'[t])^2+Izz*(θz'[t])^
2)-Ixz*θx'[t]*θz'[t];
PE=(k1/2)*((u0[t]+z1*θy[t]-y1*θz[t])^2+(v0[t]-
z1*θx[t]+x1*θz[t])^2+(w0[t]-
x1*θy[t]+y1*θx[t])^2)+(k2/2)*((u0[t]+z2*θy[t]-y2*θz[t])^2+(v0[t]-
z2*θx[t]+x2*θz[t])^2+(w0[t]-
x2*θy[t]+y2*θx[t])^2)+(k3/2)*((u0[t]+z3*θy[t]-y3*θz[t])^2+(v0[t]-
z3*θx[t]+x3*θz[t])^2+(w0[t]-
x3*θy[t]+y3*θx[t])^2)+(k4/2)*((u0[t]+z4*θy[t]-y4*θz[t])^2+(v0[t]-
z4*θx[t]+x4*θz[t])^2+(w0[t]-x4*θy[t]+y4*θx[t])^2);
(* Potential Energy of the Springs Attached to Plate*)
(* Rayleigh Dissipation Energy of the Dampers Attached to Plate*)
RD=(c1/2)*((u0'[t]+z1*θ'y[t]-y1*θz'[t])^2+(v0'[t]-
z1*θx'[t]+x1*θz'[t])^2+(w0'[t]-
x1*θy'[t]+y1*θx'[t])^2)+(c2/2)*((u0'[t]+z2*θy'[t]-
y2*θz'[t])^2+(v0'[t]-z2*θx'[t]+x2*θz'[t])^2+(w0'[t]-
x2*θy'[t]+y2*θx'[t])^2)+(c3/2)*((u0'[t]+z3*θy'[t]-
y3*θz'[t])^2+(v0'[t]-z3*θx'[t]+x3*θz'[t])^2+(w0'[t]-
x3*θy'[t]+y3*θx'[t])^2)+(c4/2)*((u0'[t]+z4*θy'[t]-
y4*θz'[t])^2+(v0'[t]-z4*θx'[t]+x4*θz'[t])^2+(w0'[t]-
x4*θy'[t]+y4*θx'[t])^2);
eqn[i_]:=D[D[(KE1+KE2+KE),velocity[[i]]],t]-
D[(KE1+KE2+KE),position[[i]]]+D[(RD1+RD2+RD),velocity[[i]]]+D[(PE
1+PE2+PE),position[[i]]];
Stiffness=Table[Coefficient[eqn[j],position[[k]]],{k,9},{j,9}];
Mass=Table[Coefficient[eqn[j],acceleration[[k]]],{k,9},{j,9}];
Damping=Table[α*Mass[[j,k]]+β*Stiffness[[j,k]],{k,9},{j,9}];
```

```
L=Chop[CholeskyDecomposition[Mass]];
MD1=Inverse[Transpose[L]].Mass.Inverse[L];
KD1=Inverse[Transpose[L]].Stiffness.Inverse[L];
CD1=Inverse[Transpose[L]].Damping.Inverse[L];
FD1=Chop[Inverse[Transpose[L]].F];
vecs=Chop[Eigenvectors[KD1]];
P=Transpose[vecs];
Ptranspose = vecs;
S=Inverse[L].P;
KD2 =Chop[Ptranspose.KD1.P];
MatrixForm[%];
MD2 =Chop[Ptranspose.MD1.P];
MatrixForm[%];
CD2 =Chop[Ptranspose.CD1.P];
MatrixForm[%];
FD2=Chop[Simplify[Ptranspose.FD1]]
MatrixForm[%];
particular11=Table[Coefficient[FD2[[j]],Sin[ω11*t]],{j,9}];
particular12=Table[Coefficient[FD2[[j]],Sin[ω12*t]],{j,9}];
particular13=Table[Coefficient[FD2[[j]],Sin[ω13*t]],{j,9}];
particular14=Table[Coefficient[FD2[[j]],Sin[ω14*t]],{j,9}];
particular15=Table[Coefficient[FD2[[j]],Sin[ω15*t]],{j,9}];
particular16=Table[Coefficient[FD2[[j]],Sin[ω16*t]],{j,9}];
particular17=Table[Coefficient[FD2[[j]],Sin[ω17*t]],{j,9}];
MatrixForm[%];
particular21=Table[Coefficient[FD2[[j]],Sin[ω21*t]],{j,9}];
particular22=Table[Coefficient[FD2[[j]],Sin[ω22*t]],{j,9}];
particular23=Table[Coefficient[FD2[[j]],Sin[ω23*t]],{j,9}];
particular24=Table[Coefficient[FD2[[j]],Sin[ω24*t]],{j,9}];
particular25=Table[Coefficient[FD2[[j]],Sin[ω25*t]],{j,9}];
particular26=Table[Coefficient[FD2[[j]],Sin[ω26*t]],{j,9}];
particular27=Table[Coefficient[FD2[[j]],Sin[ω27*t]],{j,9}];
MatrixForm[%];
vals=Chop[Eigenvalues[KD1]];
ωn=Sqrt[vals];
ζ=(α/(2*ωn))+(β*ωn)/2;
ωd=Table[ωn[[j]]*Sqrt[1-ζ[[j]]],{j,9}];
fn=Sqrt[vals]/(2*Pi);
fd=ωd/(2*Pi);
{23.71629340343848` (Sin[11.09` t]+Sin[21.77` t]+Sin[24.88`
t]+Sin[32.76` t]+Sin[41.99` t]+Sin[47.93` t]+Sin[60.22`
t])+12.176380963697648` (Sin[5.99` t]+Sin[12.08` t]+Sin[16.45`
t]+Sin[35.` t]+Sin[43.12` t]+Sin[47.08` t]+Sin[75.`
t]),0.47429779935456384` (Sin[11.09` t]+Sin[21.77` t]+Sin[24.88`
t]+Sin[32.76` t]+Sin[41.99` t]+Sin[47.93` t]+Sin[60.22`
t])+28.545273262255563` (Sin[5.99` t]+Sin[12.08` t]+Sin[16.45`
t]+Sin[35.` t]+Sin[43.12` t]+Sin[47.08` t]+Sin[75.` t]),-
23.912619107296337` (Sin[11.09` t]+Sin[21.77` t]+Sin[24.88`
t]+Sin[32.76` t]+Sin[41.99` t]+Sin[47.93` t]+Sin[60.22`
```

```
t])+13.049440953020028` (Sin[5.99` t]+Sin[12.08` t]+Sin[16.45`
t]+Sin[35.` t]+Sin[43.12` t]+Sin[47.08` t]+Sin[75.` t]),-
0.055967219247049844` (Sin[11.09` t]+Sin[21.77` t]+Sin[24.88`
t]+Sin[32.76` t]+Sin[41.99` t]+Sin[47.93` t]+Sin[60.22` t])-
1.511881440302727` (Sin[5.99` t]+Sin[12.08` t]+Sin[16.45`
t]+Sin[35.` t]+Sin[43.12` t]+Sin[47.08` t]+Sin[75.`
t]),2.2775481852129817` (Sin[11.09` t]+Sin[21.77` t]+Sin[24.88`
t]+Sin[32.76` t]+Sin[41.99` t]+Sin[47.93` t]+Sin[60.22` t])-
1.8192557459641425` (Sin[5.99` t]+Sin[12.08` t]+Sin[16.45`
t]+Sin[35.` t]+Sin[43.12` t]+Sin[47.08` t]+Sin[75.`
t]),0.31869739985449297` (Sin[11.09` t]+Sin[21.77` t]+Sin[24.88`
t]+Sin[32.76` t]+Sin[41.99` t]+Sin[47.93` t]+Sin[60.22` t])-
0.08118442721821306` (Sin[5.99` t]+Sin[12.08` t]+Sin[16.45`
t]+Sin[35.` t]+Sin[43.12` t]+Sin[47.08` t]+Sin[75.` t]),-
0.1684652471422208` (Sin[11.09` t]+Sin[21.77` t]+Sin[24.88`
t]+Sin[32.76` t]+Sin[41.99` t]+Sin[47.93` t]+Sin[60.22`
t])+0.828263591485338` (Sin[5.99` t]+Sin[12.08` t]+Sin[16.45`
t]+Sin[35.` t]+Sin[43.12` t]+Sin[47.08` t]+Sin[75.`
t]),0.23605585449666983` (Sin[11.09` t]+Sin[21.77` t]+Sin[24.88`
t]+Sin[32.76` t]+Sin[41.99` t]+Sin[47.93` t]+Sin[60.22`
t])+3.008949946399901` (Sin[5.99` t]+Sin[12.08` t]+Sin[16.45`
t]+Sin[35.` t]+Sin[43.12` t]+Sin[47.08` t]+Sin[75.`
t]),4.289741825716503` (Sin[11.09` t]+Sin[21.77` t]+Sin[24.88`
t]+Sin[32.76` t]+Sin[41.99` t]+Sin[47.93` t]+Sin[60.22`
t])+3.087057744212988` (Sin[5.99` t]+Sin[12.08` t]+Sin[16.45`
t]+Sin[35.` t]+Sin[43.12` t]+Sin[47.08` t]+Sin[75.` t])}
(*Displacement Solution - Each solution will be a superposition
of two solutions because od the two forcing functions*)
X11=Table[particular11[[n]]/Sqrt[(ωn[[n]]^2-
ω11^2)^2+(2*ζ[[n]]*ωn[[n]]*ω11)^2],{n,1,9}];
θ11=Table[ArcTan[(2*ζ[[n]]*ωn[[n]]*ω11)/(ωn[[n]]^2-
ω11^2)],{n,1,9}];
X12=Table[particular12[[n]]/Sqrt[(ωn[[n]]^2-
ω12^2)^2+(2*ζ[[n]]*ωn[[n]]*ω12)^2],{n,1,9}];
θ12=Table[ArcTan[(2*ζ[[n]]*ωn[[n]]*ω12)/(ωn[[n]]^2-
ω12^2)],{n,1,9}];
X13=Table[particular13[[n]]/Sqrt[(ωn[[n]]^2-
ω13^2)^2+(2*ζ[[n]]*ωn[[n]]*ω13)^2],{n,1,9}];
θ13=Table[ArcTan[(2*ζ[[n]]*ωn[[n]]*ω13)/(ωn[[n]]^2-
ω13^2)],{n,1,9}];
X14=Table[particular14[[n]]/Sqrt[(ωn[[n]]^2-
ω14^2)^2+(2*ζ[[n]]*ωn[[n]]*ω14)^2],{n,1,9}];
θ14=Table[ArcTan[(2*ζ[[n]]*ωn[[n]]*ω14)/(ωn[[n]]^2-
ω14^2)],{n,1,9}];
X15=Table[particular15[[n]]/Sqrt[(ωn[[n]]^2-
ω15^2)^2+(2*ζ[[n]]*ωn[[n]]*ω15)^2],{n,1,9}];
θ15=Table[ArcTan[(2*ζ[[n]]*ωn[[n]]*ω15)/(ωn[[n]]^2-
ω15^2)],{n,1,9}];
```

```
X16=Table[particular16[[n]]/Sqrt[(ωn[[n]]^2-
ω16^2)^2+(2*ζ[[n]]*ωn[[n]]*ω16)^2],{n,1,9}];
θ16=Table[ArcTan[(2*ζ[[n]]*ωn[[n]]*ω16)/(ωn[[n]]^2-
ω16^2)],{n,1,9}];
X17=Table[particular17[[n]]/Sqrt[(ωn[[n]]^2-
ω17^2)^2+(2*ζ[[n]]*ωn[[n]]*ω17)^2],{n,1,9}];
θ17=Table[ArcTan[(2*ζ[[n]]*ωn[[n]]*ω17)/(ωn[[n]]^2-
ω17^2)],{n,1,9}];
X21=Table[particular21[[n]]/Sqrt[(ωn[[n]]^2-
ω21^2)^2+(2*ζ[[n]]*ωn[[n]]*ω21)^2],{n,1,9}];
θ21=Table[ArcTan[(2*ζ[[n]]*ωn[[n]]*ω21)/(ωn[[n]]^2-
ω21^2)],{n,1,9}];
X22=Table[particular22[[n]]/Sqrt[(ωn[[n]]^2-
ω22^2)^2+(2*ζ[[n]]*ωn[[n]]*ω22)^2],{n,1,9}];
θ22=Table[ArcTan[(2*ζ[[n]]*ωn[[n]]*ω22)/(ωn[[n]]^2-
ω22^2)],{n,1,9}];
X23=Table[particular23[[n]]/Sqrt[(ωn[[n]]^2-
ω23^2)^2+(2*ζ[[n]]*ωn[[n]]*ω23)^2],{n,1,9}];
θ23=Table[ArcTan[(2*ζ[[n]]*ωn[[n]]*ω23)/(ωn[[n]]^2-
ω23^2)],{n,1,9}];
X24=Table[particular24[[n]]/Sqrt[(ωn[[n]]^2-
ω24^2)^2+(2*ζ[[n]]*ωn[[n]]*ω24)^2],{n,1,9}];
θ24=Table[ArcTan[(2*ζ[[n]]*ωn[[n]]*ω24)/(ωn[[n]]^2-
ω24^2)],{n,1,9}];
X25=Table[particular25[[n]]/Sqrt[(ωn[[n]]^2-
ω25^2)^2+(2*ζ[[n]]*ωn[[n]]*ω25)^2],{n,1,9}];
θ25=Table[ArcTan[(2*ζ[[n]]*ωn[[n]]*ω25)/(ωn[[n]]^2-
ω25^2)],{n,1,9}];
X26=Table[particular26[[n]]/Sqrt[(ωn[[n]]^2-
ω26^2)^2+(2*ζ[[n]]*ωn[[n]]*ω26)^2],{n,1,9}];
θ26=Table[ArcTan[(2*ζ[[n]]*ωn[[n]]*ω26)/(ωn[[n]]^2-
ω26^2)],{n,1,9}];
X27=Table[particular27[[n]]/Sqrt[(ωn[[n]]^2-
ω27^2)^2+(2*ζ[[n]]*ωn[[n]]*ω27)^2],{n,1,9}];
θ27=Table[ArcTan[(2*ζ[[n]]*ωn[[n]]*ω27)/(ωn[[n]]^2-
ω27^2)],{n,1,9}];
rxp=Chop[Table[X11[[k]]*Sin[ω11*t+θ11[[k]]]+X12[[k]]*Sin[ω12*t+θ
12[[k]]]+

X13[[k]]*Sin[ω13*t+θ13[[k]]]+X14[[k]]*Sin[ω14*t+θ14[[k]]]+X15[[k
]]*Sin[ω15*t+θ15[[k]]]+X16[[k]]*Sin[ω16*t+θ16[[k]]]+X17[[k]]*Sin
[ω17*t+θ17[[k]]]+
     +X21[[k]]*Sin[ω21*t+θ21[[k]]]+X22[[k]]*Sin[ω22*t+θ22[[k]]]+
```

```
X23[[k]]*Sin[ω23*t+θ23[[k]]]+X24[[k]]*Sin[ω24*t+θ24[[k]]]+X25[[k
]]*Sin[ω25*t+θ25[[k]]]+X26[[k]]*Sin[ω26*t+θ26[[k]]]+X27[[k]]*Sin
[ω27*t+θ27[[k]]],{k,1,9}]];
Sinverse=Ptranspose.L;


xx=Chop[S.rxp];
us11=xx[[1]];
vs11=xx[[2]];
vs22=xx[[3]];
u0=xx[[4]];
v0=xx[[5]];
w0=xx[[6]];
ϕx=xx[[7]];
ϕy=xx[[8]];
ϕz=xx[[9]];
plotfs1x=Plot[F[[1]],{t,0,tf},PlotStyle→Thin,PlotRange→All,Plot
Label→Subscript["F",1],AxesLabel→{secs,lb}];
plotfs1y=Plot[F[[3]],{t,0,tf},PlotStyle→Thin,PlotRange→All,Plot
Label→Subscript["F",2],AxesLabel→{secs,lb}];
plotfs2y=Plot[F[[3]],{t,0,tf},PlotStyle→Thin,PlotRange→All]
Show[plotfs1x,plotfs1y,plotfs2y]
plotu0=Plot[u0,{t,0,tf},PlotStyle→Thin,PlotRange→All,PlotLabel→
Subscript[u,0],AxesLabel→{secs,ft}]
plotv0=Plot[v0,{t,0,tf},PlotStyle→Thin,PlotRange-
>All,PlotLabel→Subscript[v,0],AxesLabel→{secs,ft}]
plotw0=Plot[w0,{t,0,tf},PlotStyle→Thin,PlotRange→All,PlotLabel→
Subscript[w,0],AxesLabel→{secs,ft}]
plotϕx=Plot[ϕx,{t,0,tf},PlotStyle→Thin,PlotRange→All,PlotLabel→
Subscript[θ,x],AxesLabel→{secs,rads}];
plotϕy=Plot[ϕy,{t,0,tf},PlotStyle→Thin,PlotRange→All,PlotLabel→
Subscript[θ,y],AxesLabel→{secs,rads}];
plotϕz=Plot[ϕz,{t,0,tf},PlotStyle→Thin,PlotRange→All,PlotLabel→
Subscript[θ,z],AxesLabel→{secs,rads}];
Show[GraphicsArray[{{plotu0,plotϕx},{plotv0,plotϕy},{plotw0,plotϕ
z}}]]
```